UNIVERSITY OF GAZİANTEP
GRADUATE SCHOOL OF
NATURAL & APPLIED SCIENCES

DESIGN AND COMPUTER SIMULATION ON MULTI-EFFECT EVAPORATION SEAWATER DESALINATION SYSTEM USING HYBRID RENEWABLE ENERGY SOURCES IN TURKEY

M. Sc. THESIS
IN
MECHANICAL ENGINEERING

BY
İBRAHİM HALİL YILMAZ
JULY 2009

Design and Computer Simulation on Multi-Effect Evaporation Seawater Desalination System Using Hybrid Renewable Energy Sources in Turkey

M.Sc. Thesis
in
Mechanical Engineering
University of Gaziantep

Supervisor
Prof. Dr. M. Sait SÖYLEMEZ

by

İbrahim Halil YILMAZ

July 2009

T.C.
UNIVERSITY OF GAZİANTEP
GRADUATE SCHOOL OF
NATURAL & APPLIED SCIENCES
MECHANICAL ENGINEERING

Name of the thesis: Design and Computer Simulation on Multi-Effect Evaporation Seawater Desalination System Using Hybrid Renewable Energy Sources in Turkey
Name of the student: İbrahim Halil YILMAZ
Exam date: 23.07.2009

Approval of the Graduate School of Natural and Applied Sciences

(Prof. Dr. Ramazan KOÇ)
Director

I certify that this thesis satisfies all the requirements as a thesis for the degree of Master of Science.

(Prof. Dr. Sedat BAYSEÇ)
Head of Department

This is to certify that we have read this thesis and that in our opinion it is fully adequate, in scope and quality, as a thesis for the degree of Master of Science.

(Prof. Dr. M. Sait SÖYLEMEZ)
Supervisor

Examining Committee Members	Signature
Prof. Dr. Ali Rıza TEKİN (Chairman)	_____
Prof. Dr. M. Sait SÖYLEMEZ	_____
Prof. Dr. Mehmet KANOĞLU	_____

ABSTRACT

Design and Computer Simulation on Multi-Effect Evaporation Seawater Desalination System Using Hybrid Renewable Energy Sources in Turkey

YILMAZ, İbrahim Halil
M.Sc. in Mechanical Eng.
Supervisor: Prof. Dr. M. Sait SÖYLEMEZ
July 2009, 82 pages

The present work outlines the design and computer simulation on Multi-Effect Evaporation Forward-Feed (MEE-FF) seawater desalination system using hybrid Renewable Energy Sources (solar and wind) in Turkey. It will serve as a feasibility and applicability study on Multi-Effect Evaporation seawater desalination system in 18 stations. A simulation program was built in Visual Basic programming language in order to perform this study. Hourly values of solar radiation flux on horizontal surface, ambient temperatures, wind velocities and seawater temperatures which have been measured for ten years (1997 to 2007) used for 18 stations, have taken from the Turkish State Meteorological Service to obtain more reliable and realistic simulation results. Mathematical modelings of MEE-FF seawater desalination system, flat-plate collector and wind turbine were made. The system model includes the basic thermodynamics laws, continuity equations, heat transfer equations and the thermodynamics relations. A system was designed and the design criteria for all sub-systems were developed for providing the interconnections among these sub-systems. Simulation results of the developed mathematical models were compared with literature and yielded satisfactory results. On the other hand, the feasibility comparisons of the stations were made from the point of renewable energy potential. Mersin and Çanakkale had the highest solar energy and wind energy potential, respectively among 18 stations.

Keywords: Multi-Effect Evaporation system, seawater desalination, hybrid renewable energy sources, flat-plate collector, wind turbine

ÖZET

Türkiye'de Hibrit Yenilenebilir Enerji Kaynaklarının Kullanımıyla Çok Kademeli Buharlaştırma Deniz suyunu Tuzundan Arındırma Sistemi Üzerine Tasarım ve Bilgisayar Simülasyonu

YILMAZ, İbrahim Halil
Yüksek Lisans Tezi, Makine Müh. Bölümü
Tez Yöneticisi: Prof. Dr. M. Sait SÖYLEMEZ
Temmuz 2009, 82 sayfa

Bu çalışma, Türkiye'de hibrit yenilenebilir enerji kaynaklarının (güneş ve rüzgâr) kullanımıyla Çok Kademeli Buharlaştırma İleri-Beslemeli (ÇKB-İB) deniz suyunu tuzundan arındırma sistemi üzerine tasarım ve bilgisayar simülasyonunu kapsamaktadır. Çok Kademeli Buharlaştırma deniz suyunu tuzundan arındırma sistemi üzerine 18 istasyon'da fizibilite ve uygulanabilirlik çalışması olarak görev yapacaktır. Bu çalışmayı gerçekleştirecek bir simülasyon programı Visual Basic programlama diliyle meydana getirilmiştir. Daha güvenilir ve gerçekçi simülasyon sonuçları elde edebilmek için, 18 istasyon'da (1997 den 2007)'ye kadar ölçülen saatlik yatay yüzeye düşen güneş ışınım değerleri, dış ortam sıcaklıkları, rüzgâr hızları ve deniz suyu sıcaklıkları Devlet Meteoroloji İşleri Genel Müdürlüğünden alınmıştır. ÇKB-İB deniz suyunu tuzundan arındırma sistemi, düz plakalı kolektör ve rüzgâr türbininin matematik modelleri oluşturulmuştur. Sistem modeli temel termodinamik kanunları, süreklilik denklemleri, ısı transfer denklemleri ve termodinamik ilişkileri içermektedir. Bir sistem tasarımı yapıldı ve alt-sistemleri arasında ara-bağlantıyı sağlayacak tasarım kıstasları geliştirildi. Geliştirilen matematik modellerinin simülasyon sonuçları literatür ile kıyaslanıp, tatmin edici sonuçlar alınmıştır. Öte yandan, istasyonların fizibilite kıyaslamaları yenilebilir enerji potansiyelleri açısından yapılmıştır. 18 istasyon arasında, Mersin ve Çanakkale en yüksek güneş enerjisi ve rüzgâr enerjisi potansiyeline sırasıyla sahip olmuştur.

Anahtar kelimeler: Çok Kademeli Buharlaştırma sistemi, deniz suyunu tuzundan arındırma, hibrit yenilebilir enerji kaynakları, düz plakalı kolektör, rüzgâr türbini.

ACKNOWLEDGEMENTS

I express my appreciation to my supervisor Prof. Dr. M. Sait SÖYLEMEZ for his guidance during completion of the thesis.

I would like to give special thanks to my friend of troublesome; Electric & Electronic Engineer Ergün MENETLİOĞLU who contributed many efforts in developing the simulation program and much improving its quality.

I would like to serve my gratitude to examining committee members spending their valuable time for attending my M.Sc. qualification.

I would like to thank Assoc. Prof. Dr. Recep YUMRUTAŞ and Assist. Prof. Dr. Önder KAŞKA as well, for their suggestions and encouragement during the progress of the thesis.

Many thanks also to my colleagues Emrah ÖZAHİ, Ali KILIÇ and dear teacher Raziye KAZANCI to give valuable advices to me.

I couldn't find the right expressions to say my family but I would like to thank for showing their valuable sacrifice in every stage of the study.

And finally thanks to someone who wasn't getting named here but he participated in any part of this thesis.

CONTENTS

LIST OF FIGURES

LIST OF SYMBOLS

A_c	gross collector area, m²
A_{dc}	condenser area, m²
A_e	evaporator area, m²
A_p	preheater area, m²
A_r	wind turbine rotor area, m²
b_0	incidence angle modifier coefficient
$\dot{B}$	brine mass flowrate, kg/s
c_p	specific heat at constant pressure, kj/kg°C
$c_{p,w}$	specific heat of water at constant pressure, J/kg K
$\dot{d}_f$	flashed off vapor mass flowrate, kg/s
$\dot{D}$	evaporated vapor mass flowrate, kg/s
F_R	collector heat removal factor
g	gravity constant, m/s²
G_{sc}	solar constant, W/m²
h_b	equivalent head to pump rejected brine, m
h_{cw}	equivalent head to pump cooling seawater, m
h_d	equivalent head to pump distilled water, m
h_{fg}	latent heat of vaporization, kj/kg°C
h'_{fg}	latent heat of vaporization at T', kj/kg°C
h_{sw}	equivalent head to pump seawater, m
I	hourly total radiation on a horizontal surface, MJ/m²
I_0	hourly extraterrestrial radiation on a horizontal surface, MJ/m²
I_b	hourly beam radiation on a horizontal surface, MJ/m²
I_d	hourly diffuse radiation on a horizontal surface, MJ/m²

I_T	hourly total radiation on a tilted surface, MJ/m²
k_T	hourly clearness index
$K_{\tau\alpha}$	incidence angle modifier
$\dot{m}_b$	rejected brine mass flowrate, kg/s
$\dot{m}_c$	collector mass flow rate, kg/s
$\dot{m}_{cw}$	cooling seawater mass flowrate, kg/s
$\dot{m}_d$	distillate water mass flowrate, kg/s
$\dot{m}_f$	feed seawater mass flowrate, kg/s
$\dot{m}_{fv,i}$	mass flowrate of water entering flash vessel, kg/s
$\dot{m}_{fv,o}$	condensate mass flowrate outgoing from flash vessel, kg/s
$\dot{m}_s$	heating steam mass flowrate, kg/s
$\dot{m}_v$	vacuumed air mass flowrate, kg/s
$\dot{m}_w$	wind mass flowrate, kg/s
n	number of effects
N	day of the year
p_{cpi}	pressure at the collector pump inlet, Pa
p_{cpo}	pressure at the collector pump outlet, Pa
p_{co}	saturated pressure at collector outlet design temperature, Pa
P_0	standard sea level atmospheric pressure, Pa
P_{aux}	power required to auxiliary heater, W
P_{bp}	power required to drive rejected brine pump, W
P_{cp}	power required to drive collector pump, W
P_{cwp}	power required to drive cooling seawater pump, W
P_{dp}	power required to drive distilled water pump, W
P_e	electrical power output,W
P_{req}	total power required to drive all power consuming devices, W
P_{swp}	power required to drive seawater pump, W
P_w	total wind power,W

$\dot{Q}_c$	total volume flowrate entering collector array, m^3/s
Q_u	hourly useful energy gain of collector, W
R_a	specific gas constant for air, J/kg.K
R_b	geometric factor
T_a	ambient temperature, °C
T_a	ambient temperature at altitude *z*, K
T_c	condensation temperature, °C
T_c'	flashing condensation temperature, °C
T_{ci}	collector fluid inlet temperature, °C
T_{co}	collector fluid outlet temperature, °C
T_{co}	collector outlet design temperature, °C
T_{cw}	cooling seawater temperature, °C
T_f	feed seawater temperature, °C
T_i	boiling temperature in effect i, °C
T_i'	flashing temperature in effect i, °C
$T_{lp,o}$	outlet temperature of flash vessel condensate from last preheater, °C
T_p	preheating temperature, °C
$T_{o,\#s}$	outlet temperature of the series' last collector, °C
T_v	vapor saturation temperature, °C
U_c	condenser overall heat transfer coefficient, $kW/m^2°C$
U_e	evaporator overall heat transfer coefficient, $kW/m^2°C$
U_{lp}	last preheater overall heat transfer coefficient, $kW/m^2°C$
U_L	overall heat loss coefficient, W/m^2 K
U_p	overall heat transfer coefficient of preheater, $kW/m^2°C$
X	brine salt concentration, ppm
X_b	rejected brine salt concentration, ppm
X_d	distillate water salt concentration, ppm
X_f	feed seawater salt concentration, ppm

z	altitude above sea level, m
z_0	reference altitude, m
(BPE)	boiling point elevation, °C
(NEA)	non-equilibrium allowance, °C
Δp	pressure difference, Pa
Δp_{cl}	pressure drop across inlet and outlet of a single collector, Pa
ΔT_{bl}	bundle losses, °C
ΔT_y	hydrostatic pressure head, °C
$(\Delta T_{lm})_c$	logarithmic mean temperature difference at condenser, °C
$(\Delta T_{lm})_{lp}$	logarithmic mean temperature difference at the last preheater, °C
$(\Delta T_{lm})_p$	logarithmic mean temperature difference at preheater, °C

Greek letters

β	slope of collector, deg
γ	surface azimuth angle, deg
δ	declination angle, deg
θ	incidence angle of beam radiation, deg
θ_z	zenith angle, deg
ϕ	latitude angle, deg
ω	hour angle, deg
ω_1, ω_2	hour angles at the start & the end of the hour, deg
ρ_a	air density, kg/m³
ρ_g	diffuse ground reflectance
$\rho(z)$	air density as a function of altitude, kg/m³
v_w	wind velocity, m/s
v_z	predicted wind speed at altitude z, m/s
v_0	wind speed at altitude z_0, m/s
$(\tau\alpha)$	transmittance-absorptance product for the glazing
$(\tau\alpha)_n$	normal transmittance-absorptance product for the glazing

Dimensionless

c_P	wind turbine power coefficient
c_{PR}	wind turbine rotor power coefficient
η_{bp}	rejected brine pump efficiency
η_c	instantaneous efficiency of collector
η_{cp}	collector pump efficiency
η_{cw}	cooling seawater pump efficiency
η_{dc}	down condenser thermal efficiency
η_{dp}	distilled water pump efficiency
η_g	total electrical efficiency of wind turbine
η_{lp}	last preheater thermal efficiency
η_m	total mechanical efficiency of wind turbine
η_p	preheater thermal efficiency
η_{swp}	seawater pump efficiency

Subscripts

ave	average
c	condensation
cr	condensate steam return
i	effect number
j	preheater number
k	collector number connected parallel
n	last effect
s	steam
sat	saturated
v	vapor
$\#s$	number of collector connected series

CHAPTER 1

INTRODUCTION

Water scarcity has constituted a remarkable problem in many part of the world. Increasing in global temperature causes more water to be evaporated from sources hence it leads unavoidably deficiency of water around the world. When global temperature more increases gives rise to decreasing in the quantity of potable water sources and contrarily increasing in the fresh water need. If some precautions are not taken, the problem will probably threat us in near future. The most reasonable approach to the solution of fresh water supply appears to be desalting of seawater. It is known that oceans and inland seas contain nearly 97.5 percent of earth's water and this can be potable if its saline content is reduced.

All the desalting processes definitely require energy to remove or purify salts from seawater. If desalination is accomplished by conventional technology, then it will require burning of substantial quantities of fossil fuels. However the researches made recently illustrate that fossil fuels will deplete in near future roughly 200 years afterwards. Using up these sources leads us to find executable alternative energy sources such as renewable energy in order to overcome this problem.

Renewable energy systems produce energy from sources that are naturally replenished and inexhaustible. Production of fresh water using desalination technologies driven by renewable energy systems is thought to be a viable solution where availability of the resources is high. Despite the fact that renewable energy is inexhaustible, by its nature, it tends to be intermittent and variable in intensity character associated to major problems with technical challenge. Thus, the obvious way is to couple renewable energy sources with desalination processes in order to take the advantages of both and become a promising solution for these limitations. Furthermore all desalination processes or energy supply

systems from renewable sources or their combinations may not be feasible technically and economically for all locations. To overcome these problems, a simulation program is required for evolving process configuration for a specified location before setting up a system. There is no available software which is commercially or educational based user-friendly for designing and analyzing desalination system and renewable energy systems together, and then evaluating the locations in Turkey for interconnecting renewable energy sources with desalination plant. In order to fulfill this gap, user-friendly software has been prepared and presented herein.

A software package is developed for design, simulation and analysis of Multi-Effect Evaporation Forward-Feed (MEE-FF) desalination with the renewable energy sources of solar and wind. Visual Basic programming language is used due to its flexibility and user-interface. The software uses the site meteorological solar, wind, ambient temperature and seawater temperature data regarding to the station of the meteorology. It presents to user its simplicity in the software structure and ergonomics. It has also the graphic-wizard application built by ActiveX control.

This thesis includes chapters on the study of Design and Computer Simulation on Multi-Effect Evaporation Seawater Desalination System Using Hybrid Renewable Energy Sources in Turkey. The flow diagram of the designed system is illustrated in Figure (1.1). The desalination part is focused on the analysis of multi-effect evaporation sub-system. The energy supplement via hybrid renewable energy resources are followed by solar and wind powered sub-systems. Design and computer simulation are realized with using the software, Visual Basic. It is noted that complete and detailed description are made for all the sub-systems processes. The content of each chapter is presented briefly as below.

In Chapter 2, related studies occupied in the literature are briefly described. The studies are collected under two sections which are simulation and mathematical models and solar-sourced practiced multi-effect distillation systems. The first section includes mostly the studies on steady-state mathematical models of the Multi-Effect desalination systems and the simulation programs peculiar to their model predictions and codes. The second section includes the practiced Multi-Effect desalination

systems that are sourced by solar as a renewable energy using different types of solar collector systems.

In Chapter 3, feasibility and applicability of a MEE desalination unit powered with solar energy are determined. The suitability of the process with respect to renewable energy source and the corresponding desalination system selection are explained. The developed process description and the flow-diagram of the desalination sub-system are presented. And also the system analysis and the mathematical modeling equations are covered to build the software computing algorithm.

In Chapter 4, supplying of the thermal energy required for the desalination sub-system is defined. The selection of a suitable collector type for the desalination process and the required criteria for the system feasibility are examined. The mathematical modeling of the Flat-plate collector and the task is to be accomplished by the collector arrangement's design are developed. Accordingly, the suitable method for steam generation is selected as steam-flash concept whose design parameters and mathematical modeling are expressed.

In Chapter 5, the electrical power, which is required by the overall system, supplied via wind turbine is determined. The model assumptions and design considerations are taken into account within subsequent sections. The power needed by all the system components are defined as a result sizing the wind power system is to provide this need considered as regards the sub-system design criteria.

In Chapter 6, the working principle of the simulation program called as RES Hybridized MEE Seawater Desalting System Simulator is presented. The program panel, its tab mode and the procedure is to be applied to the sub-systems are explained in the sections of the chapter in a detailed manner. The simulation results obtained are monitored in the software. The simulation graphics devoted to the sub-systems and overall system are being drawn in last tab of the package and the obtained results can be analyzed and compared with literature.

In Chapter 7, the conclusions and recommendations related with system simulation are summarized.

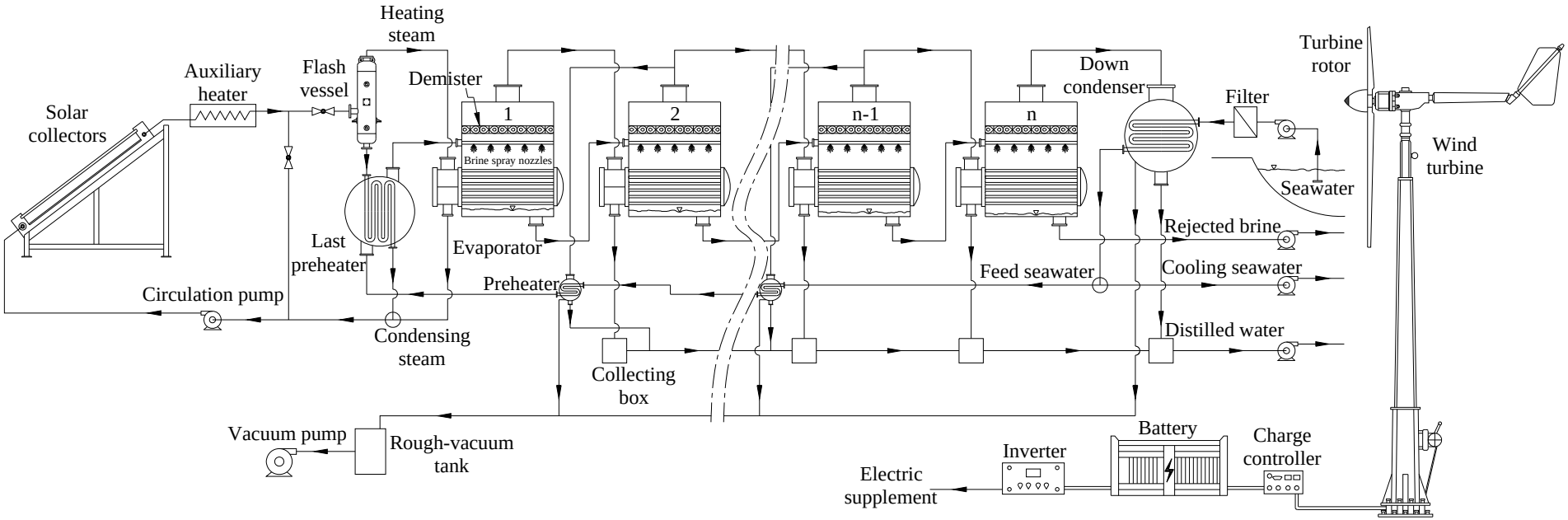

Figure 1.1 The flow diagram of MEE-FF seawater desalination system using hybrid RES

CHAPTER 2

LITERATURE REVIEW

2.1 Introduction

As it is deduced from the studies and research made in the literature in recent times, there have been developed many simulation software packages on Multi-Effect desalination systems. On the other hand, a large number of research institutes, industries and researchers apply serious effort to develop solar energized desalination plants. Nevertheless there has not been any study made on the ME system hybridized with solar and wind energies.

It is obvious from the literature review that there is a need to develop a software for designing an appropriate ME desalination process-combination powered with solar and wind energy sourced sub-systems while selecting a geographical location (in Turkey) regarding with its specific site parameters. Hence, in this thesis, a computer simulation program is developed to analyze the geographical location evaluating the interconnection between desalination and renewable energy sourced sub-systems. The analyses of the simulation results illustrate the feasibility on the locations to choice the most appropriate one where the system is monitored for utilizing the solar/wind resources of the site.

2.2 Studies on Simulation and Mathematical Modeling of Multi-Effect Distillation Systems

El-Dessouky et al. [1] developed an efficient and accurate mathematical modeling based on the analysis of the steady state mass and heat balances coupled with the heat transfer rate equations for each individual effect of MEE desalination

process. The model assumes the practical case of constant heat transfer areas for both the evaporators and feed preheaters in all effects. The system modeling determines the effects of the important design and operating variables on the parameters controlling the cost of producing fresh water. Design correlations were also developed to describe variations in performance parameters of the desalination unit in terms of the top brine temperature and the number of effects.

Aly and El-Fiqi [2] described a steady-state mathematical model developed to analyze both the multi-stage and multi-effect desalination systems. For MED, the effect of the process variables on the performance parameters of a “forward type” multi-effect boiling falling film was carried out.

Darwish et al. [3] revisited the conventional multi-effect desalting system making a simple analysis of forward feed with feed heaters. It was indicated that thermal energy input to LTME (Low Temperature Multi Effect) in the range of 70°C is low, and can bring the equivalent mechanical energy, and thus the consumed fuel energy, to low values.

Ettouney and El-Dessouky [4] developed a computer package for design and simulation of thermal desalination processes. The package includes models for various systems of single effect evaporation (SEE), multistage flash (MSF), and multi effect evaporation (MEE) including parallel and forward feed systems configurations. All models are based on a well developed set of materials and energy balance equations as well as correlations for evaluation of physical properties, heat transfer coefficient, and thermodynamic losses. All mathematical models developed and previously tested and validated by the authors against available industrial and literature data. The computer package includes the displays for process design, rating, flow charting, performance calculations, help files, and graphing of process schematics and performance curves. The reported results for various systems are consistent with literature data and industrial practice.

Ettouney [5] developed a visual basic computer package for the design and analysis of thermal and membrane desalination processes. The package includes conventional processes, i.e., multiple-effect evaporation with/without thermal or

mechanical vapor compression. The model predictions are based on detailed energy and material balances and well tested correlations for the heat transfer coefficient, thermodynamic losses, and physical properties of the seawater and water vapor. The simulator gives the user efficient tools for system design or simulation. Displays for the process flow diagram and design results are generated simultaneously. The package integrates well with other literature attempts focusing on developing a package for process simulation or cost estimation.

Nafeya et al. [6] developed a VDS (Visual Design & Simulation) package for design and simulation of different types and configurations of desalination processes. Object-oriented programming with Visual Basic was used to simulate some operating desalination plants to offer a flexible reliable and friendly user-interface. Typical desalination processes such as multistage flash, multi-effect evaporation, thermal vapor compression, mechanical vapor compression and reverse osmosis were simulated to show the wide scope and great capability of the package. The capability of the developed VDS package was examined by performing a design calculation of a large-scale MEE desalination plant with a heat recovery system. The design of a ten-effect evaporation system with heat recovery by intermediate condensing and vapor bleeding was considered. Validity of the VDS package demonstrated a satisfactory agreement between the calculated results and the referenced results.

Jernqvista et al. [7] have developed a general computer code whose advanced graphic capabilities enable the user to construct process flow sheets on the screen, for all types of evaporation and flashing processes. The program was designed to be very flexible and can be used as an excellent tool for the simulation, rating and optimization of all types of thermal desalination processes.

2.3 Studies on Solar-Sourced Practiced Multi-Effect Distillation Systems

Delyannis [8] overviewed some of the solar assisted desalination plants. A small seawater solar desalination pilot plant was implemented by Sasakura Eng. Co. at Takami Island in Japan. The system had multi-effect stack (MES) distillation

concept whose capacity of 16 m³/day. The thermal energy requirement of the system was provided by flat-plate collectors.

Abu-Jabal et al. [9] presented a practical scale desalination system of three effects using only solar energy from solar collectors as the heat source and the electrical power from the PV cells. The unit was developed and manufactured by the Ebara Corporation (Tokyo) and the Water Research Center in Al Azhar University is performing the tests for the system. The unit is considered as a zero-brine-discharge system, and the desalination method is evaporation distillation with triple-effect evaporators; basically it is a batch process for every-day operation with brackish water. The study describes the unit, discusses the method used for distillation and results of the tests during the testing period. It also shows the feasibility of using the system in the region.

El-Nashar [10] reviewed a small seawater solar desalination plant's design concept which had been designed and constructed as part of a cooperative research program for solar desalination between the Water and Electricity Department (Abu Dhabi) and the New Energy Development Organisation (Japan) and also presented the results of two preliminary performance simulation models. The system utilized the horizontal-tube, thin-film, multi-effect stack (MES) distillation concept and had a design capacity of 120 m³/day. The thermal energy required by the MES evaporator was provided by a bank of evacuated glass tube collectors. The system used no auxiliary heat with solar energy representing the only source of thermal energy. The solar collectors had an effective area of 1862 m^2. Three thermally stratified vertical thermal storage tanks with a total capacity of 300 m^3 were utilized to provide thermal energy for the distiller. The plant was designed for continuous operation day and night.

Kalogirou [11] analysed the various desalination methods with respect to their primary energy consumption, sea-water treatment requirement and equipment cost. From this analysis, the multiple-effect boiling evaporator was concluded to be the most suitable method for stimulation by solar energy. The parabolic-trough solar-collector was selected mainly due to its ability to function at high temperatures with

high efficiency. The design of the flash vessel and the desalination system circuit also were presented in the study.

Milowr and Zarza [12] demonstrated the Solar Thermal Desalination (STD) project proving that seawater solar desalination with MED plants is a good alternative for medium to large fresh water production systems. The technical feasibility and high reliability of an MED plant coupled to a solar parabolic-trough collector field. From 1988 until 1994, the Plataforma Solar de Almeria developed a unique experience in the desalination of sea water with solar energy. The system developed that has a production capacity of 72 m^3/d and still running.

CHAPTER 3

DESIGN & ANALYSIS OF MEE DESALTING SUB-SYSTEM

3.1 Introduction

Multi-effect evaporation (MEE) is one of the main and oldest thermal desalination method. But since 1960 Multi-stage Flash (MSF) process dominated the desalination market. Recent developments in MEE technology have again brought it to the point of competing technically and economically with MSF process. MEE has a number of distinguished features, in particular, lower primary energy consumption, higher gain output ratio, lower heat transfer area [13]. MEE process is less susceptible to corrosion and scaling than the MSF process [14]. These features are important for the development of an economically feasible small-scale desalination unit powered with solar energy. This explains why small-scale thermal desalination units designed in the last few years were based on the MEE process.

3.2 Multi-Effect Evaporation Desalting Systems

The multiple effect evaporation desalting systems can be configured in forward, backward, or parallel feed. These three configurations differ in the flow directions of the heating-steam and the evaporating brine [1].

The backward-feed arrangement has some of the disadvantages over the other MEE desalting systems. The major disadvantage in the backward system; the increase in the pumping power, maintenance cost, and the increase in air leakage point through pump connections. The second one is that the temperature-concentration profile crosses the solubility limits for the calcium sulfate and this makes the process inapplicable in seawater desalination [15].

The parallel feed layout is by no means the most economical and is efficient only when the feed brine is nearly saturated to begin boiling inside the effects. The salt concentration reaches the maximum permissible value in all effects. Therefore, the parallel configuration is very appropriate for low top-brine temperature design.

In the forward-feed system, both the brine and the heating steam flow concurrently from the high temperature to the lower temperature effect. The concentration of the evaporated brine increases from the first effect to the last. The layout advantage is the absence of pumps for moving or rejecting brine from the effects. It has the disadvantage that all the feed has to be heated to the boiling temperature before boiling commences. In other words, one part of the heating steam when condensed does not accomplish any evaporation in the first or consecutive effects; thus, less vapor is generated from the heating steam, which lowers the performance ratio. Furthermore, the most concentrated brine is subjected to the coolest temperature, which reduces the heat transfer coefficient because of the viscosity increase. However, at the same time, this reduces the rate of scale formation. All these facts make the system very suitable for high temperature application.

3.3 Seawater Desalination System Selection

During the design, there is a need to select a process suitable for a particular application. The factors to be considered during such a selection are [11]:

- Suitability of the process to solar-energy application.
- The effectiveness of the process with respect to energy consumption.
- The amount of fresh water required in a particular application in combination with the range of applicability of the various desalination-processes.
- The sea-water treatment requirements.
- The capital cost of the equipment.
- The land area required, or could be made available, for the installation of the equipment.

According to [11,1], the MEE requires less specific energy, is cheaper and requires only a very simple sea-water treatment when compared with the MSF. In addition, MEE exhibits various advantages when compared with other distillation processes:

- Energy economy as the brine is not heated to above its boiling-point as in the MSF process. This leads to inherently less irreversibility in the MEE process as the vapor is used at the temperature at which it is generated.
- The feed is at its lowest concentration at the highest plant temperature, so that scale formation risks are minimized.
- The feed flows through the plant in series and, as the maximum concentration only occurs at the last effect, the worst boiling-point elevation is confined to this effect.
- The other processes have high electrical demands, because of the recirculation pump in the MSF or the vapor compressor in the Vapor Compression (VC) systems.
- MSF is prone to equilibrium problems, which reflect themselves in a reduction in PR. In MEE plants, the vapor generated in one effect, is used in the next and PR is not subject to equilibrium problems.
- Plant simplicity is promoted by the MEE process as less effects are required to give a certain PR.

Therefore, the MEE process appears to be the most suitable if it is used with solar energy as a renewable energy source [11].

3.4 Process Description

Figure 3.1 shows the process diagram of the Multiple-Effect Evaporation Forward-Feed (MEE-FF) seawater desalination system which consists of effects arranged in series. The system has n number of evaporators, a series of feed seawater preheaters, equal to $n-1$, a train of collecting boxes, equal to n, a down condenser, and a vacuum system. Each effect contains heat exchange tubes, vapor space, brine spray nozzles and mist eliminator. The horizontal falling film evaporator is preferred

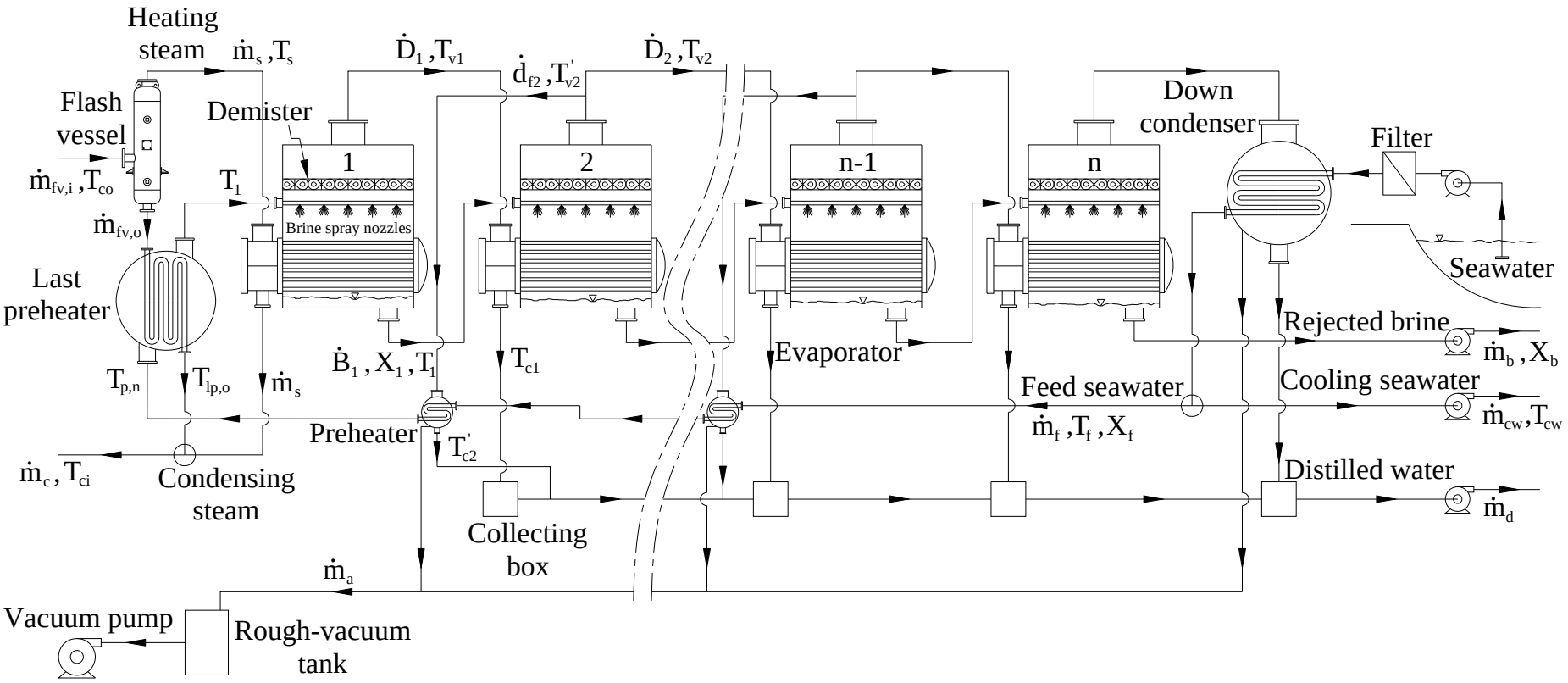

Figure 3.1 Process diagram of the MEE-FF seawater desalination system

to use in the MEE desalination processes because of having remarkable advantages [15].

In the forward-feed configuration, the flow direction of the brine and vapor is in the lowering pressure which is gradually reduced from effect 1 to *n*. The feed seawater flows from effect 1 to *n* and the steam generated with steam-flash concept, enters the first effect and is condensed to boil the pre-heated feed seawater to produce vapor, is used as heating medium to generate steam in the downstream effect. This permits the feed seawater to undergo multiple boiling without supplying additional heat after the first effect. This process is repeated all the way down to the last effect. The condensates coming from the effects except the first are collected at collecting boxes as product water.

The intake seawater flows into the down condenser with a flowrate of $\dot{m}_{cw} + \dot{m}_f$ which absorbs the latent heat of vapors formed (evaporating and flashing) in the effect *n*. The seawater stream is heated from the intake temperature, T_{cw} to a higher temperature, T_f. The excess heat loaded to the system is removed by the cooling seawater, $\dot{m}_{cw}$ at the down condenser. After rejecting the cooling seawater back to the sea, the feed seawater, $\dot{m}_f$, is chemically treated, deaerated, and pumped through a series of preheaters. Preheating of the feed seawater is made by flashed-off vapors, $\dot{d}_{f,i}$ coming from the effects. And the feed water enters the last preheater then leaves it at top brine temperature, T_1 corresponding to the saturated pressure in the first effect and is sprayed over the heat exchanger tubes. However, there is no flashed-off vapor within the first effect owing to no temperature difference between the feed seawater and the first effect. The brine spray forms a thin film around the succeeding rows of horizontal tubes. The saturation temperature of the formed vapor, $T_{v,1}$ is less than the brine boiling temperature by the boiling point elevation, $(BPE)_1$. A small part of the feed water is evaporated, $\dot{D}_1$ just by boiling in the first effect. The vapor produced flows through a knitted wire mist eliminator known as wire mesh demister to remove the entrained brine droplets and then undergoes to boil some part of the feed, left from the first effect ($\dot{m}_f - \dot{D}_1$), in the second effect which

is maintained at a lower pressure than the former. Moreover vapor is formed after the first effect process by flashing as well. Flashing takes place in effects 2 through n due to the fact that the brine temperature flowing from the previous effect, T_{i-1} is higher than the saturation temperature of the next effect, $T_{v,i}$. Therefore, vapor flashes to provide the effect equilibrium thermodynamically. This situation causes to form the some part of the thermodynamic losses such that non-equilibrium allowance $(NEA)_i$, which is a measure of the efficiency of the flashing process, in effects 2 to n. Thus, the boiling temperature within the effect, T_i, is lower than the temperature of flashing brine, $T_i^{'}$, by the non-equilibrium allowance $(NEA)_i$. Furthermore reduction in the vapor temperature is also caused by bundle losses which include frictional losses in the demister, transmission lines, gravity and deceleration.

3.5 System Analysis

The MEE-FF desalination unit is presented in a detailed mathematical model. The assumptions made to build the model do not sacrifice far from the actual systems. The system model includes the basic thermodynamics laws, continuity equations, heat transfer equations and the thermodynamics relations. The main characteristics of the model include the followings:

- It maintains constant heat transfer areas in evaporators and feed heaters. This is common industrial practice, which is necessary to reduce cost of construction, spare parts stocking, and maintenance [1].
- It includes the variations in the thermodynamic losses such as (BPE) and (NEA) for each effect.
- It takes into account variation of seawater specific heat at constant pressure with temperature and salinity and also water physical properties as a function of temperature such as specific heat at constant pressure, latent heat of vaporization, saturation pressure and saturated liquid enthalpy.
- It includes the variation of overall heat transfer coefficient of evaporators and down condenser as a function of effect vapor temperatures.

Assumptions that made in the model include the following approaches:

- All the system components perform under the steady state conditions. As a matter of fact that due to the variation in solar radiation fluxes during the day lead the system operates at unsteady condition. However the auxiliary heating system provides the plant operate under the steady state.
- Distillate product collected at the collecting boxes is salt free.
- Heat losses to the surroundings are negligible because the system components are well insulated and operate at relatively low temperatures between 100-40°C.
- Bundle losses for each effect are assumed to be constant because the design dimensions of the system components are not known.
- In contrast to evaporators and down condenser, preheaters have constant overall heat transfer coefficient.
- Thermal efficiency of heat exchange units is assumed constant.
- The rate of non-condensable venting is fixed to 0.5% of the vapor flow entering into each effect [7].

3.6 Process Modeling

The continuity equation to desalination unit under steady-state assumption is simplified to the form written below. The feed seawater flowrate is equal to the sum of the distillate and rejected brine flow rates.

$$\dot{m}_f = \dot{m}_d + \dot{m}_b \tag{3.1}$$

The salt concentration balance is given by Eq. (3.2)

$$X_f \dot{m}_f = X_d \dot{m}_d + X_b \dot{m}_b \tag{3.2}$$

Thus, the distillate water is salt free, $X_d = 0$ the equation is simplified to

$$\dot{m}_b = \dot{m}_f \frac{X_f}{X_b} \tag{3.3}$$

The total distillate flowrate is defined as the amounts of vapor formed by boiling and flashing within the effects.

$$\dot{m}_d = \sum_{i=1}^{n} \dot{D}_i + \sum_{i=2}^{n} \dot{d}_{f,i} \tag{3.4}$$

The brine flow rate leaving the first effect is given by the difference between the feedwater and the amount of vapor formed in the first effect.

$$\dot{B}_1 = \dot{m}_f - \dot{D}_1 \tag{3.5}$$

The brine mass flowrate leaving each effect is given in Eq. (3.6)

$$\dot{B}_i = \dot{m}_f - \sum_{i=1}^{n} \dot{D}_i - \sum_{i=2}^{n} \dot{d}_{f,i} \tag{3.6}$$

The salt concentration of the brine leaving the first effect,

$$X_1 = \frac{\dot{m}_f X_f}{\dot{B}_1} \tag{3.7}$$

The salt concentration values from effect 2 to *n* are calculated by the Eq. (3.8) with the same way,

$$X_i = \frac{\dot{m}_f X_f}{\dot{B}_i} \tag{3.8}$$

The energy balance relation for the first effect requires that the latent heat supplied by the heating steam is absorbed by the boiled vapor at the effect vapor temperature.

$$\dot{m}_s h_{fg,s} = \dot{D}_1 h_{fg,v1} \tag{3.9}$$

where the correlation for the latent heat of vaporization is given in Appendix A.

The vapor temperature of aqueous solution is less than pure water at the same pressure. Thus the boiling temperature of seawater will be higher than that of the water by the boiling point elevation. On the other hand, the temperature rise at the boiling temperature caused by the hydrostatic pressure head, $\Delta T_{y,i}$, is negligible in horizontal falling films, because of the very small thickness of the boiling film [1].

$$T_i = T_{v,i} + (BPE)_i + \Delta T_{y,i} \tag{3.10}$$

where the correlation for the boiling point elevation of seawater is given in Appendix A.

The vapor boiled in the first effect transfers its latent heat to the vapor will be evaporated in the next effect. The energy balance relation becomes

$$\dot{D}_i = \frac{\dot{D}_{i-1} h_{fg,c(i-1)}}{h_{fg,vi}} \tag{3.11}$$

After the boiling process take places on the outer surface of the evaporator tubes, the condensation temperature, T_{ci}, falls down to the effect temperature, T_i, as a result of thermodynamic losses such as boiling point elevation and bundle losses.

$$T_{ci} = T_i - (BPE)_i - (\Delta T_{bl})_i \tag{3.12}$$

When the brine of the first effect enters the second effect, which is at a lower temperature, it suddenly flashes and consequently its temperature is reduced from T_i to T_i' as much as non-equilibrium allowance until the thermal equilibrium is attained.

$$T_i' = T_i + (NEA)_i \tag{3.13}$$

The correlation for the non-equilibrium allowance in the MEE process is given in [1].

$$(NEA)_i = \frac{33\Delta T_i^{0.55}}{T_{vi}}$$

where $\Delta T_i = T_{i-1} - T_i$, is temperature difference of boiling brine in effects i and $i-1$, T_{vi} is the vapor temperature in effect i.

The flashing process composes of a small part of the distillate for the corresponding effect. The energy balance for this process is evaluated at the second effect.

$$\dot{d}_{f,2} = \left(\dot{m}_f - \dot{D}_1\right) c_{p,ave} \frac{T_1 - T_2'}{h'_{fg,v2}} \tag{3.14}$$

Similar processes occur within the effects 3 to n, the energy balance is turned to the Eq. (3.15).

$$\dot{d}_{f,i} = \left(\dot{m}_f - \sum_{i=1}^{n} \dot{D}_i - \sum_{i=2}^{n} \dot{d}_{f,i} \right) c_{p,ave} \frac{T_{i-1} - T_i'}{h'_{fg,vi}} \tag{3.15}$$

The vapors formed by boiling and flashing in the last effect increases the temperature of the intake seawater, $\dot{m}_f + \dot{m}_{cw}$, from T_{cw} to T_f within the down condenser.

$$\eta_{dc}\left(\dot{d}_{f,n} h'_{fg,cn} + \dot{D}_n h_{fg,cn}\right) = \left(\dot{m}_f + \dot{m}_{cw}\right) c_{p,ave}\left(T_f - T_{cw}\right) \tag{3.16}$$

The heat transfer surface area of the evaporators can be determined from the Equation (3.17) through the effects of 1 to *n*.

$$A_{e,i} = \frac{\dot{m}_s h_{fg,s}}{U_{e1}\left(T_s - T_1\right)} = \frac{\dot{D}_i h_{fg,vi}}{U_{ei}\left(T_{c(i-1)} - T_i\right)} \tag{3.17}$$

Determining the down condenser area, the log mean temperature difference (LMTD) method is very suitable in heat exchanger analysis when the mass flow rates and the inlet and outlet temperatures of the hot and cold fluids are specified [16].

$$A_{dc} = \frac{\left(\dot{m}_f + \dot{m}_{cw}\right)c_{p,ave}\left(T_f - T_{cw}\right)}{U_c\left(\Delta T_{lm}\right)_c} \tag{3.18}$$

where $\left(\Delta T_{lm}\right)_c = \dfrac{\Delta T_1 - \Delta T_2}{\ln\left(\Delta T_1 / \Delta T_2\right)}$

ΔT_{lm} is the log mean temperature difference. Here ΔT_1 and ΔT_2 represent the temperature difference between the fluids at the inlet and outlet of the down condenser.

The condenser can be treated as a counter-flow heat exchanger since the temperature of the heating vapor remains constant. The temperature difference between the vapor and the cooling seawater at the two ends of the condenser becomes equal to $\Delta T_1 = T'_{cn} - T_{cw}$ and $\Delta T_2 = T'_{cn} - T_f$.

The vapors formed by flashing in the effects increase the temperature of the feed seawater passing the preheater *j* through *n*-1 to 2.

$$\eta_p \dot{d}_{f,j} h'_{fg,cj} = \dot{m}_f c_p \left(T_{n-2} - T_{n-1}\right) \tag{3.19}$$

Similarly, the following relation gives the calculation of heat transfer area in the preheater *j* through *n*-1 to 2.

$$A_{p,j} = \frac{\dot{m}_f c_{p,sw}\left(T_{p,n-2} - T_{p,n-1}\right)}{U_p\left(\Delta T_{lm}\right)_p} \tag{3.20}$$

The preheating process can be treated as counter-flow manner since the temperature of the flashing vapor remains constant during the condensation. The temperature difference between the vapor and the feedwater at the two ends of the preheaters become equal to $\Delta T_1 = T'_{cj} - T_{p,n-1}$ and $\Delta T_2 = T'_{cj} - T_{p,n-2}$.

After calculating the heat transfer areas for each evaporator and preheater, as common industrial practice, they are getting equaled to a constant area that is the averaged of the calculated areas for the evaporators and preheaters separately.

CHAPTER 4

DESIGN & ANALYSIS OF SOLAR ENERGIZED SUB-SYSTEM

4.1 Introduction

A solar collector is a special kind of heat exchanger that converts solar radiant energy to thermal energy. The working fluid in the collector is heated by the solar flux as it passes through the collector tubes. The energy gained by this renewable source is utilized to produce the heating steam required by desalination unit.

The main solar collectors suitable for seawater distillation process are given in [17] as follow: flat-plate collectors (FPC), evacuated tube collectors (ETC), compound parabolic collectors (CPC) and parabolic trough collectors (PTC).

4.2 Collector Type Selection

The selection of a suitable collector type for a given application takes into account definite advantages when it is analyzed from the view of system design, its feasibility and the required criteria [17]. The preceding factors were examined in the selection of flat-plate type collector as compared with the other collector types as follow:

- Flat-plate collectors are in wide use for hot-water heating where the demand temperature is not high, i.e. about 100 °C. Their usages, from the aspect of the system selection, require preheating the working fluid within the collector so that this makes the method feasible when they are applied to generate steam in accordance with the steam-flash concept.

- A flat-plate collector absorbs both the direct and the diffuse components of solar radiation. Concentrating collectors accumulate little diffuse solar irradiance depending on the concentration ratio.
- Flat-plate collectors will absorb energy coming from all directions above the absorber (both beam and diffuse solar irradiance). Because of this characteristic, flat-plate collectors do not need to track the sun. They receive more solar energy than a similarly oriented concentrating collector, but when not tracked, have greater cosine losses.
- Sun tracking is not required since flat-plate collectors may be firmly fixed to a mounting structure, and rigid plumbing may be used to connect the collectors to the remainder of the system. Moving structure, motors, and tracking control systems are eliminated, thereby reducing the complexity of the system.
- Currently, flat-plate collectors cost is less than concentrating collectors. Part of reason is the lack of need for a complex tracking system. However, part of the reason is because much more flat-plate collectors are being produced than concentrating collectors today.

4.3 Model Assumptions of the Selected Collector Type

Assumptions and design criteria made in the modeling of flat-plate collector include the followings:

- The meteorological data used in solar collector sub-system are hourly-changing and regarding to the last 10 years. The data used in the system analysis are averaged of the last 10-years to normalize the system design reflecting the all-years characteristics.
- The collector system operates under the steady-state conditions.
- Performance parameters of collectors are evaluated in accordance with ASHRAE 93 Standard specifications.
- Number of collector is to be connected in series determined according to the design criterion that takes into account the maximum useful gain taking place in the day of year.

- All collectors connected series and parallel display similar performance characteristics.

4.4 Mathematical Modeling of Flat-Plate Collector

The mathematical model developed is intended to predict the useful energy gained by the collector and correspondingly determine the outlet temperatures of the collectors in series. The model equations are given as follow:

Declination angle δ is found from the Equation (4.1)

$$\delta = 23.45 \sin\left(360 \frac{284 + N}{365}\right) \tag{4.1}$$

The equation, relating the angle of incidence of beam radiation, θ is

$$\begin{aligned}\cos\theta = {} & \sin\delta\sin\phi\cos\beta - \sin\delta\cos\phi\sin\beta\cos\gamma + \cos\delta\cos\phi\cos\beta\cos\omega \\ & + \cos\delta\sin\phi\sin\beta\cos\gamma\cos\omega + \cos\delta\sin\beta\sin\gamma\sin\omega\end{aligned} \tag{4.2}$$

The zenith angle of the sun, θ_z is given by the Equation (4.3)

$$\cos\theta_z = \sin\delta\sin\phi + \cos\delta\cos\phi\cos\beta\cos\omega \tag{4.3}$$

R_b, the ratio of the solar radiation falling on a tilted horizontal surface in the northern hemisphere is given as

$$R_b = \frac{\cos(\phi - \beta)\cos\delta\cos\omega + \sin(\phi - \beta)\sin\delta}{\cos\phi\cos\delta\cos\omega + \sin\phi\sin\delta} \tag{4.4}$$

The extra terrestrial radiation I_0 is calculated from the Equation (4.5)

$$I_0 = \frac{12\times 3600}{\pi} G_{sc}\left[1+0.033\cos\frac{360n}{365}\right]\times \left[\cos\phi\cos\delta(\sin\omega_2-\sin\omega_1)+\frac{2\pi(\omega_2-\omega_1)}{360}\sin\phi\sin\delta\right] \quad (4.5)$$

where $G_{sc} = 1367$ W/m² [18], is the energy from the sun per unit time received on a unit area of surface perpendicular to the direction of propagation of the radiation at the earth's mean distance from the sun outside of the atmosphere. Then the clearness index is defined as

$$k_T = \frac{I}{I_0} \quad (4.6)$$

The equations for the correlation to calculate diffuse radiation are given in [18]

$$\frac{I_d}{I} = \begin{cases} 1.0-0.09k_T & k_T \le 0.22 \\ 0.9511-0.1604k_T+4.388k_T^2-16.638k_T^3+12.336k_T^4 & \text{for } 0.22 < k_T \le 0.8 \\ 0.165 & k_T > 0.80 \end{cases} \quad (4.7)$$

Then beam radiation I_b is calculated as follows

$$I_b = I - I_d \quad (4.8)$$

The total solar radiation falling on the tilted surface for the period of an hour is calculated afterwards

$$I_T = I_b R_b + I_d\left(\frac{1+\cos\beta}{2}\right)+(I_b+I_d)\left(\frac{1-\cos\beta}{2}\right)\rho_g \quad (4.9)$$

where, ρ_g is 0.2 when there is no snow and 0.7 when there is a fresh snow cover.

The incident angle modifier $K_{\tau\alpha}$, defined as the ratio of $\tau\alpha$ at incidence angle θ to $\tau\alpha$ at normal radiation $(\tau\alpha)_n$, is described by the following simple expression:

$$K_{\tau\alpha} = \frac{(\tau\alpha)}{(\tau\alpha)_n} = 1 + b_0\left(\frac{1}{\cos\theta} - 1\right) \tag{4.10}$$

This equation is outlined in ASHRAE 93 Standard convention [19]. At larger angles of incidence, the linear relationship is no longer applied. Therefore, curve fitting equation of experimental test results for the incident angle modifier can be taken from manufacturer's catalogues.

The useful energy gain under steady-state conditions can be written as

$$Q_u = A_c F_R\left[I_T K_{\tau\alpha}(\tau\alpha)_n - U_L(T_i - T_a)\right] \tag{4.11}$$

The ASHRAE standard test method for collectors can be characterized by the intercept and slope as seen in the Figure (4.1). $F_R U_L$ is equal to negative slope and the intercept of the line on the η_c axis is $F_R(\tau\alpha)_n$. Experimental thermal efficiency curve parameters can be used from manufacturers' catalogues meeting ASHRAE 93 Standard specifications.

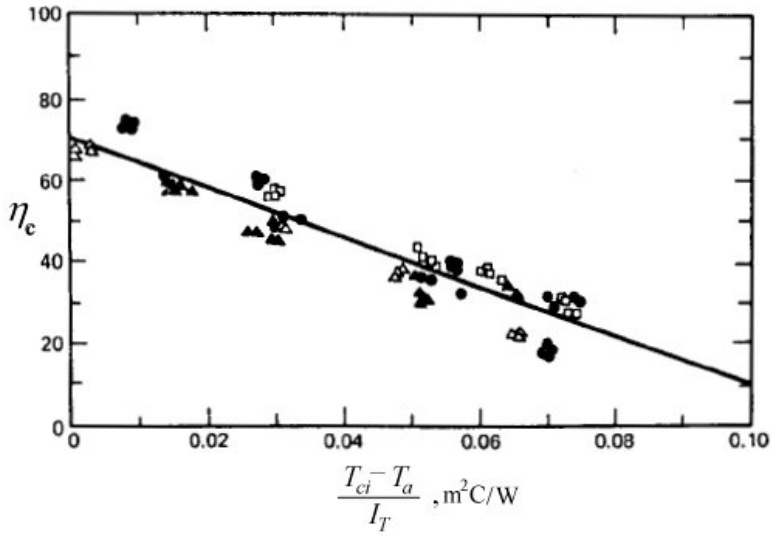

Figure 4.1 Experimental collector efficiency data measured for a liquid heating flat-plate collector

The collector inlet temperature, which is the mixing temperature of the steam condensate return temperature and the outlet temperature of flash vessel condensate from the last preheater, can be found from the energy balance.

$$T_{ci,1} = \frac{\dot{m}_{fv,o} T_{lp,o} + \dot{m}_{s,c} T_{s,cr}}{\dot{m}_c} \tag{4.12}$$

The collector outlet temperatures for collector array are given as follow:

$$T_{co,k} = \sum_{k=1}^{\#s} T_{ci,k} + \frac{Q_u}{\dot{m}_c c_{p,w}} \tag{4.13}$$

Collector modules are connected in series to increase the temperature of the collector working fluid incrementally. In series arrangement, the outlet temperature from the first collector will be the inlet to the preceding one and continue in turn with the same manner. Array characteristics for the series-connected modules are having similar $F_R(\tau\alpha)$ and $F_R U_L$ values as in the single modules. Collector modules connected in parallel increases mass flow-rate individually coming from arrays in order to provide required quantity that enters the flash vessel.

Connecting the collectors with one set of manifolds makes it difficult to ensure drainability, balanced flow, and low pressure drop. An array usually includes many individual groups of collectors, called rows, to provide the necessary flow characteristics. Parallel flow is the most frequently used because it is inherently balanced, has low pressure drop, and is drainable [20]. A sample collector configuration is shown in Figure (4.2).

Flow may be imbalanced if too many collectors are connected in parallel and pressure drop increases with raising the number of collectors. Figure (4.3) illustrates the effect of collector number on performance and pressure drop for one particular design [20]. As seen from the Fig. (4.3), when the connected collector's number increases up to a certain value, pressure drop increases remarkably. Collector parallel

arrangement is to be restricted at this limit to eliminate pressure drop arising from this effect.

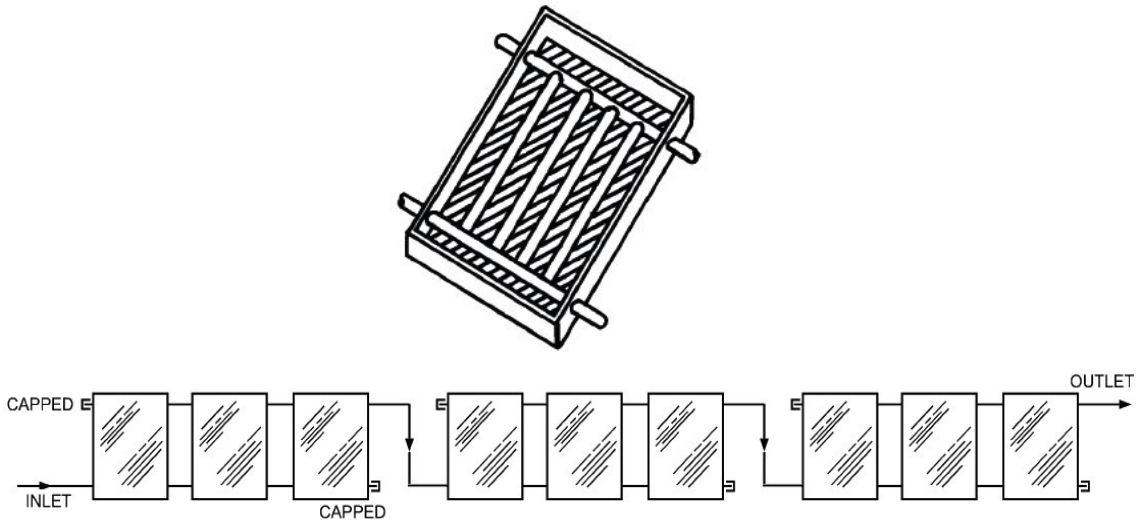

Figure 4.2 Collector manifolding arrangements for parallel-flow row

In order to prevent this problem flow restrictors can be used to accommodate a large number of collectors in a row. The flow distribution would not be satisfactory when too many collectors in parallel without the flow restrictors, which are barriers with a drilled hole, at the interconnections [20].

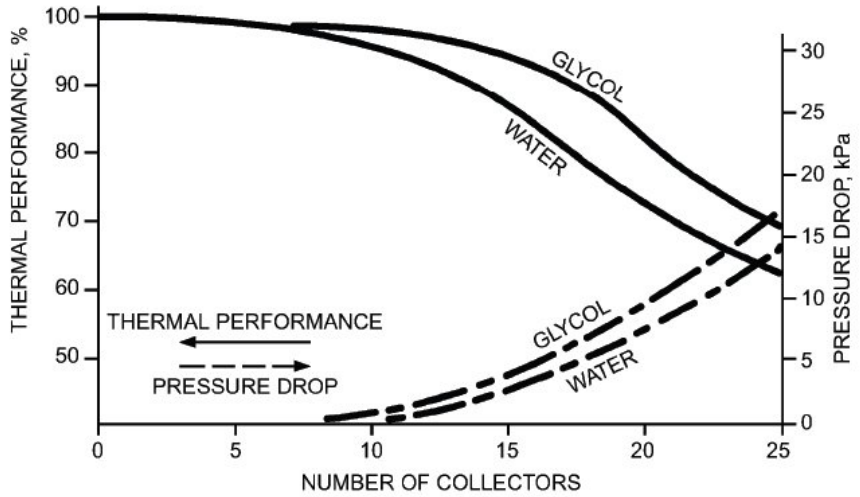

Figure 4.3 Pressure drop and thermal performance of collectors with internal manifolds numbers

The thermal performance of a collector in array that connected series can be determined from the Equation (4.14),

$$\eta_c = \frac{Q_u}{A_c I_T} = F_R(\tau\alpha) - F_R U_L \frac{(T_i - T_a)}{I_T} \tag{4.14}$$

4.5 Steam Generating System Selection

The suitable method for steam generation was selected as steam-flash concept. The preceding factors were taken into consideration in the selection of steam-flash concept as follow [11]:

- Steam-flash concept is a convenient method to produce steam when it is used for low pressure heating.
- The occurrence of flow instability, in steam mass production, is not met during the system operation.
- Scaling problem in the collector tubes can be avoided as compared to the in-situ steam generation concept.
- Flash-steam concept provides some superiorities over unfired-boiler concept which uses synthetic heat transfer oil. There are many problems associated with the use of synthetic oils such as flammability, toxicity, thermal stability and high cost.
- Capital costs associated with a direct-steam and a flash-steam system would be approximately identical.

4.6 Process Description

Figure 4.4 shows that the collector working fluid, water, is pressurized by the collector pump providing the saturation pressure corresponding to the temperature at the collector exit to prevent boiling. The circulated water within the collector array is then flashed across a pressure reducing valve, connected to the vessel inlet is spring loaded for adjustment purposes, into flash vessel. The heated water enters the vessel and evaporates some portion of it.

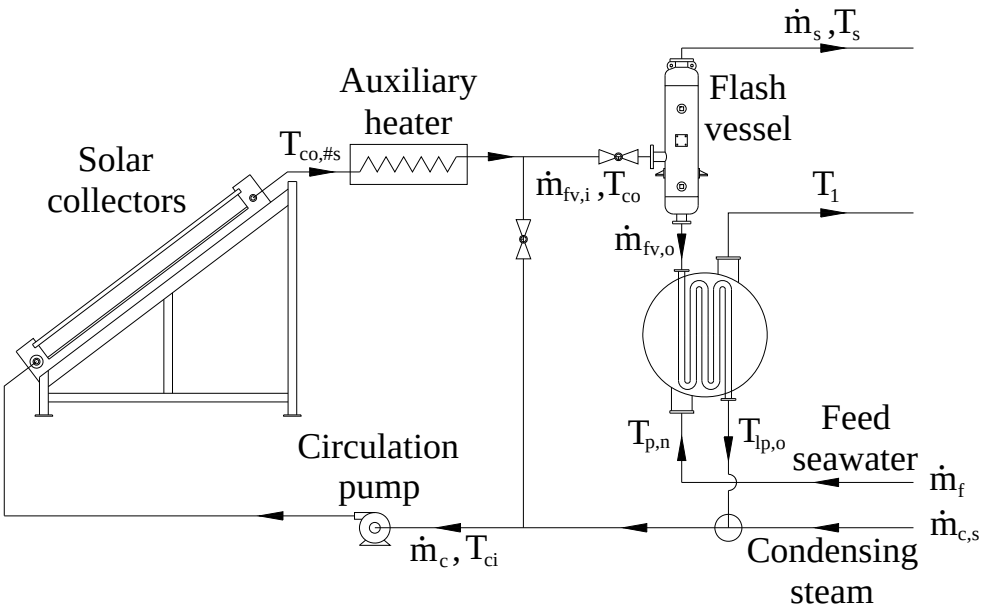

Figure 4.4 Process diagram of the solar energized sub-system

4.7 Flash-Vessel Design Parameters

Flash vessels are used to separate flash steam from condensate. Schematic representation of a flash vessel is shown in Figure (4.5). The standard design of flash vessels should ensure the followings [11]:

- The demand for flash steam should exceed its supply so that there is no build up of pressure in the flash vessel and the consequent loss of steam through the safety valve.
- A flash system generally should run at the lowest possible pressure so that the maximum amount of flash is obtainable and the backpressure on the high pressure systems is kept as low as possible.
- The diameter of the vessel is chosen to ensure drop in velocity which allows the condensate to fall to the bottom of the vessel from where it is drained out by a steam trap preferably a float trap. Flash steam itself rises to leave the vessel at the top. The height of the vessel should be sufficient enough to avoid water being carried over in the flash steam.
- The heat-up energy requirements should be kept minimal during the preheating of the flash vessel which losses its energy in the inactive time

period of the total system and this causes the vessel operating temperature return to near surrounding conditions each system start-up.

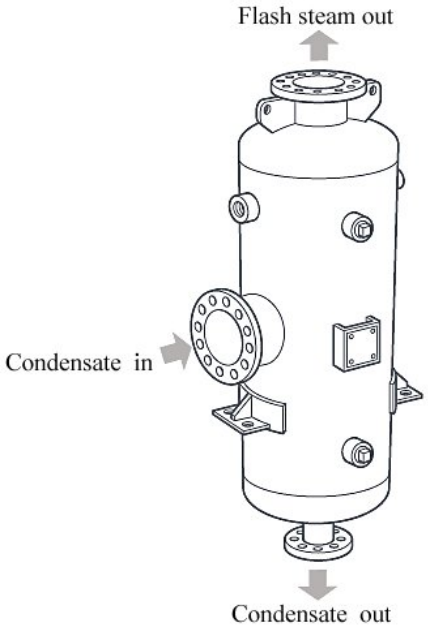

Figure 4.5 Schematic representation of a flash vessel

4.8 Mathematical Modeling of Flash Vessel

The mathematical model is developed to predict the mass flowrate of the required steam produced by the flash vessel with the help of a simple energy balance relation.

The saturated pressure at flash vessel entrance corresponds to design collector output temperature at which is the outlet of the end-collector of the series.

$$\dot{m}_s = \dot{m}_{fv,i} \frac{h_{f,e} - h_{f,i}}{h_{fg,s}} \tag{4.15}$$

where $h_{f,e}$ saturated liquid enthalpy of higher pressure condensate

$h_{f,i}$ saturated liquid enthalpy of steam at lower pressure

$h_{fg,s}$ latent heat of vaporization of flash steam at lower pressure

$\dot{m}_{fv,i}$ mass flowrate water entering into flash vessel

4.9 Last Preheater Calculations

Applying the mass conservation law under steady-state process to the flash vessel:

$$\dot{m}_{fv,o} = \dot{m}_{fv,i} - \dot{m}_s \tag{4.16}$$

The outlet temperature of flash vessel condensate at the last preheater exit is determined from the energy balance given in the Equation (4.17)

$$T_{lp,o} = T_{fv,o} - \frac{\dot{m}_f c_{p,ave}\left(T_1 - T_{p,n}\right)}{\dot{m}_{fv,o} c_{p,w}} \tag{4.17}$$

where $T_{lp,o}$ outlet temperature of flash vessel condensate from the last preheater

$T_{fv,o}$ inlet temperature of flash vessel condensate to the last preheater

T_1 outlet temperature of feed seawater from the last preheater equal to first effect temperature

$T_{p,n}$ inlet temperature of feed seawater to the last preheater

Using the log mean temperature difference (LMTD) method, the area of the last preheater can be specified as

$$A_{lp} = \frac{\dot{m}_f c_{p,ave}\left(T_1 - T_{p,n}\right)}{\eta_{lp} U_{lp} \left(\Delta T_{lm}\right)_{lp}} \tag{4.18}$$

where

$$\left(\Delta T_{lm}\right)_{lp} = \frac{\Delta T_1 - \Delta T_2}{\ln\left(\Delta T_1 / \Delta T_2\right)} \tag{4.19}$$

The last preheater is treated as a counter-flow heat exchanger so that the temperature differences are equal to $\Delta T_1 = T_{fv,o} - T_1$ and $\Delta T_2 = T_{lp,o} - T_{p,n}$, respectively.

CHAPTER 5

DESIGN & ANALYSIS OF WIND ENERGIZED SUB-SYSTEM

5.1 Introduction

A wind turbine converts the mechanical energy generated by wind to electrical energy. Wind turbines make use of the wind's kinetic energy through a system of aerodynamically shaped blades. The energy collected is transmitted as mechanical energy, which drives an electric generator, thus producing electrical power.

Wind turbines are basically classified in terms of the position of the spin axis, which can be vertical or horizontal. Horizontal-axis turbines are more generally used for electricity generation. In the analysis and the design considerations of the wind turbine, horizontal-axis turbine is considered as appropriate one to the overall system design and interconnection as shown in Figure (5.1).

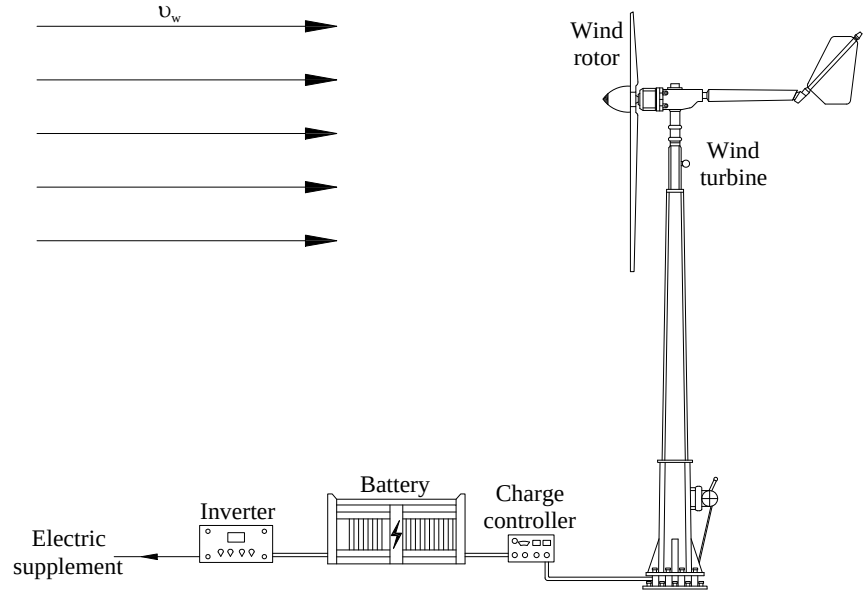

Figure 5.1 Process diagram of the wind energized sub-system

5.2 Model Assumptions

Assumptions made in the modeling of wind turbine include:

- The dependency of air density to relative humidity is ignored while the wind speeds are calculated above the sea level.
- As a design criterion, wind turbine power coefficient is considered constant during power calculations [21].
- Meteorological data for wind speeds are hourly changing in other words they are constant along the hour being involved.

5.3 Wind Energy Calculations

The total available power to a wind turbine is equal to kinetic power of the wind. The power in the wind is proportional to the air density ρ_a, the turbine rotor area A_r and the third power of the wind velocity v_w. Thus, the total wind power becomes

$$P_w = \frac{1}{2}\dot{m}_w v_w^2 = \frac{1}{2}\rho_a A_r v_w^3 \tag{5.1}$$

The maximum power that can be obtained from a wind system is 59.3 percent of the total wind power shown in [22], Appendix B. The power in the wind is converted to mechanical power with an efficiency c_{PR}, which is transmitted to the generator through a mechanical transmission with efficiency η_m and which is converted to electricity with efficiency η_g [23].

$$c_P = c_{PR}\eta_m\eta_g \tag{5.2}$$

The electrical power output is defined then

$$P_e = c_P \frac{\rho_a}{2} A_r v_w^3 \tag{5.3}$$

Optimistic values for these coefficients are $c_P = 0.45$, $\eta_m = 0.95$ and $\eta_g = 0.90$, which results the overall efficiency of 38%. Actual values will probably lie between 25% and 30% [23]. This will vary with wind speed, with the type of turbine and with the nature of load. Although the average efficiency for a typical turbine is somewhat above 20 percent, the efficiency significantly varies with the wind speed. On the other hand, power coefficient increases at high speeds so that this is a deliberate choice by the engineers who designed the turbine having high power coefficient [21]. At low wind speeds efficiency is not so important, because there is not much energy to harvest. At high wind speeds the turbine must waste any excess energy above what the generator was designed for. Hence the care must be exercised; overall efficiency should be taken in the region of high wind speeds where most of the energy is to be available.

The density of air varies with altitude and temperature. Air density decreases with altitude so that the power to be calculated must be corrected by the air density prevailing at the installation site. The change in air density is given as with a function of altitude above sea level [24].

$$\rho(z) = \frac{P_0}{R_a T_a} \exp\left(\frac{-g\,z}{R_a T_a}\right) \tag{5.4}$$

Wind speed increases with altitude when it goes away from the earth surface. Thus, knowledge of wind speeds is required to make a decision about location and rotor height of wind turbine to be installed at this altitude. These data may not be available in many times and some estimate must be made from wind speeds measured at about 10 m. The most common expression for the variation of wind speed with altitude is expressed with one-seventh power law [24].

$$v_z = v_0 \left(\frac{z}{z_0}\right)^{1/7} \tag{5.5}$$

5.4 Power Calculations

The total power required to operate the system in steady-state process is supplied by the wind turbine. Sizing the wind power system was made by considering as regards the sub-system design criterion.

- All the meteorological data used in all analysis are hourly-changing and regarding to the last 10 years. Using the data regarding to any year and designing a system with respect to this year will not indicate the all-years characteristics. Thus, the data used in the system analysis are averaged of the last 10-years to normalize the system design reflecting the all-years characteristics.
- Selecting a year that keeps the desired conditions at all times even under the worst conditions is not practical. Since such an oversized system will have a higher initial cost and will probably have a higher operating cost because the equipment in this case will run at partial load most of time and thus at a lower efficiency.
- The hourly power needed to drive all the power consuming devices is changing in each hour of the day in where all the system operates. At the times that the system is not working, the energy-storage units store the energy for the following day's system operation.

Sizing the wind turbine necessitates to be taken into account the total power required for the sub-systems of seawater desalination, solar collector and auxiliary heating. The power consumed by the system components is given as:

$$P_{req} = P_{swp} + P_{cwp} + P_{vp} + P_{bp} + P_{dp} + P_{cp} + P_{aux} \tag{5.6}$$

The power needed to pump seawater into the down condenser varies with the seawater temperature altering from day to day. Design area of condenser was determined considering a fixed seawater temperatures at the condenser inlet and outlet. Correspondingly, variation in the inlet seawater temperature on a certain day varies the mass flowrate entering the condenser, which has a constant area, changes

the required pump power. The Equation (5.7) is given as calculating the seawater pump power.

$$P_{swp} = \frac{\dot{m}_{sw} g h_{sw}}{\eta_{swp}} \tag{5.7}$$

Changing in the seawater mass flowrate accordingly changes the cooling seawater mass flowrate and then changes the power needed by pump in a parallel manner.

$$P_{cwp} = \frac{\dot{m}_{cw} g h_{cw}}{\eta_{cwp}} \tag{5.8}$$

The rate of non-condensable venting is fixed to 0.5% of the total distillate, $\dot{m}_d$. Required power is to be met from the vacuum pump for discharging of non-condensable gases, $\dot{m}_v$ taken from the manufacturers' catalogue.

The power needed to pump rejected brine back to the sea is

$$P_{bp} = \frac{\dot{m}_b g h_b}{\eta_{bp}} \tag{5.9}$$

Distillated water is pumped to where it is used and its power requirement is calculated with the same manner.

$$P_{dp} = \frac{\dot{m}_d g h_d}{\eta_{dp}} \tag{5.10}$$

The collector pump power calculation can be expressed with Bernoulli equation as in the above equations. The collector sub-system is a closed-loop system which does not require power to head the collector working fluid. The only term left from Bernoulli equation is related with static pressure to overcome collector pressure

drop when the working fluid is passing through the collector tubes. Thus, Bernoulli equation is simplified to this form:

$$P_{cp} = \frac{\Delta p \dot{Q}_c}{\eta_{cp}} = \frac{\left(p_{cpo} - p_{cpi}\right)\dot{Q}_c}{\eta_{cp}} \tag{5.11}$$

where $p_{cpo} = p_{co} + \#s \times \Delta p_{cl}$

The terms placing in the above equation are defined as

$$p_{co} = p_{sat@T_{co}} \tag{5.12}$$

and

$$p_{cpi} = p_{sat@T_{lp,o}} \tag{5.13}$$

Auxiliary power needed to heat the collector working fluid up to the collector outlet design temperature when the solar radiation is insufficient and cannot reach the collector outlet design temperature.

$$P_{aux} = \dot{m}_c c_{p,ave}\left(T_{co} - T_{o,\#s}\right) \tag{5.14}$$

CHAPTER 6

CASE STUDY

6.1 Introduction

This chapter covers how the simulation program called as RES Hybridized MEE Seawater Desalting System Simulator works. The program has a panel which collects the simulation components under its tab configuration. The software enables to user a flexible interface bringing it with tab configuration. The features collected under each tab are explained within the following sections. The program has the features, MSFlexGrid control and ActiveX control of Visual Basic infrastructure and customized ActiveX control is used in all graphic sketching interface of the program.

6.2 Station Selection

In this part of the simulation program, selection of station, where a system is to be installed, is realized. The stations are illustrated on the map of Turkey and they are located onshore as shown in Figure (6.1). Selection of station brings the data, which is to be used in the system simulation, from the created database earlier. The database is composed of the folders and they include the stations data which are mainly averaged of the last ten-year (1997/2007). The solar flux files within the radiation folder include hourly values of solar radiation flux on horizontal surface from sunrise to sunset through the days of year. The ambient temperature files have hourly values along the days of year. The wind velocity files are changing hourly along the days of year, either. The seawater temperature files are constant during the day. In addition those, the knowledge about the station latitude and salinity concentration of seawater are taken from the “Station List” file.

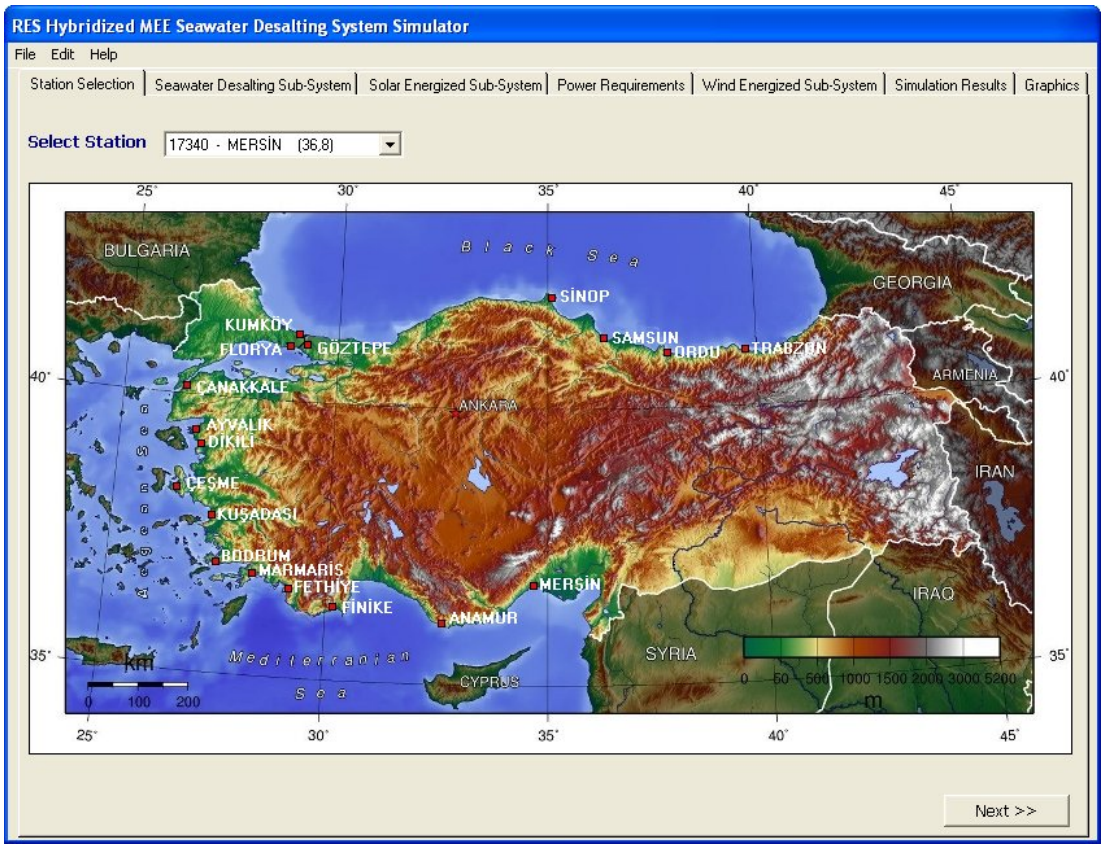

Figure 6.1 Design layout of station selection tab

6.3 Seawater Desalting Sub-System

Design of MEE-FF system tab-layout is displayed in Figure (6.2). The design data input for the desalination unit includes the parameters which make the mathematical model.

The first step is the determination of number of effect of the sub-system. Seawater salinity concentration value for the selected station is received from the database and they are quoted from the reference [25].

The instantaneous mass flow rate of the distillate product is defined to obtain the daily total distillate capacity under the steady-state conditions. Because the system total operating hour can change during day to day with variation in the renewable energy amount.

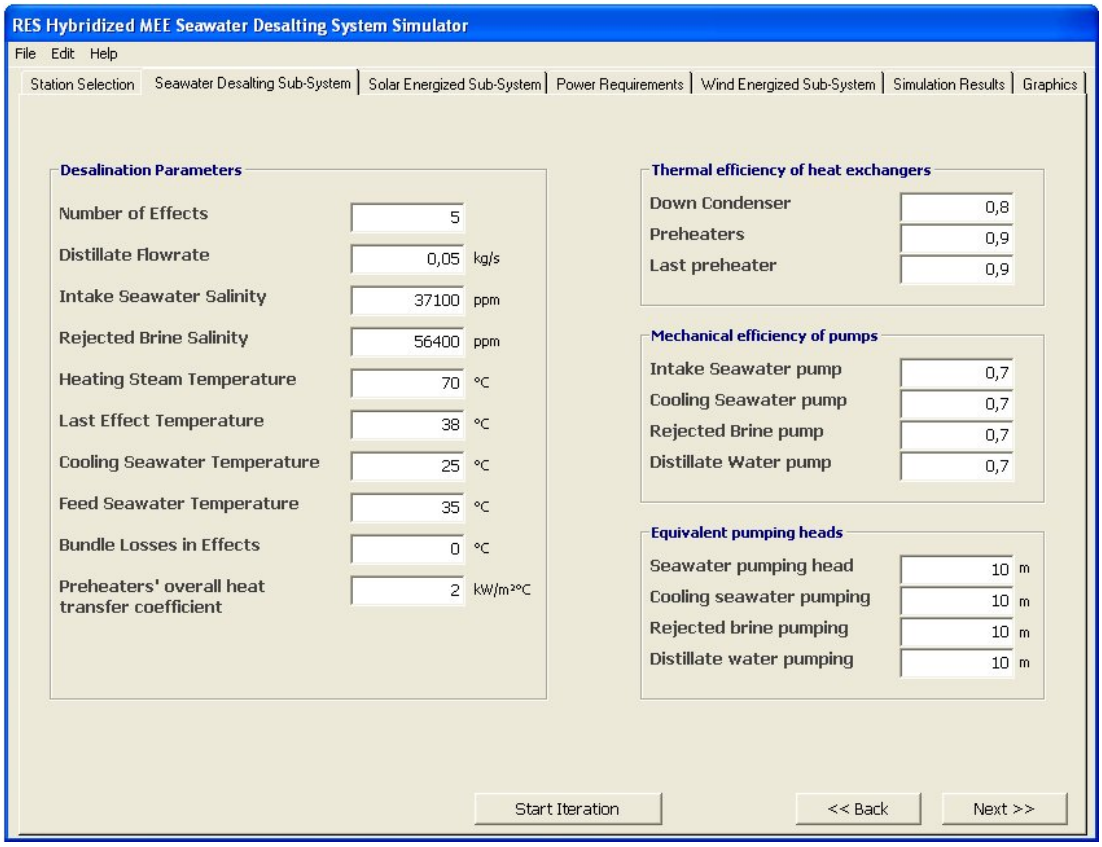

Figure 6.2 Design layout of seawater desalting sub-system tab

MEE-FF Seawater Desalination sub-system also includes the input data, the temperatures of heating steam, last effect and cooling seawater. Bundle losses and overall heat transfer coefficient are given as fixed value for effects and preheaters, respectively.

Thermal efficiency of heat exchanger, mechanical efficiency of pumps and equivalent pumping heads values are entered into the program screen as shown in Fig. (6.2).

After inputting the data for the seawater desalination sub-unit, clicking the "Start Iteration" button displays the "Iteration Parameters" window as shown in Figure (6.3). Onto this window, an initial value for the solution algorithm is required with the step size to converge the solution step rapidly. The program algorithm calculates default values for the iterating parameters. On the other hand, precision enables default values of the iteration parameters approach to the design input

parameters accurately. After iteration parameters are specified, clicking on the "Execute" button starts the iteration and continues until it is achieved.

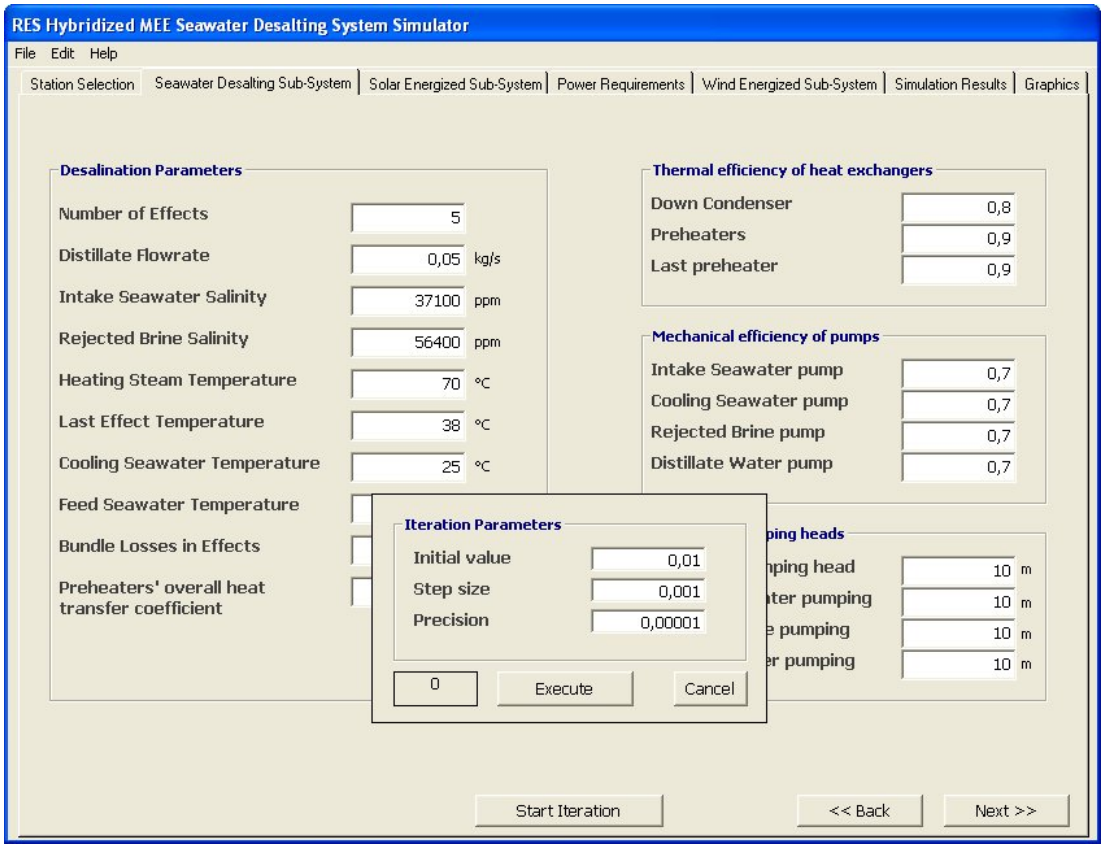

Figure 6.3 Iteration parameters window

6.4 Solar Energized Sub-System

The distribution of the daily total radiation flux over the year is illustrated in Figure (6.4) for the selected station. Flat-plate collector parameters can be selected from the pull-down box selecting an appropriate collector type which is already formed in the database. The collector models have the performance parameters according to the manufacturer's specifications which are certified by SRCC (The Solar Rating & Certification Corporation). The simulation program also provides to user entering directly the flat-plate collector parameters into the text-boxes. On the other hand, the geometrical parameters are required to design a collector under different position states.

There are two design criteria for the solar energy sub-system. One of them is

the collector outlet temperature which helps defining the series number of collector in array. The number of collector connected series is determined according to this criterion that takes into account maximum useful gain occur within the year. The second criterion is the design min-temperature which restricts the collector outlet temperature remaining under a defined value and correspondingly determines the potential days from the aspect of solar energy availability.

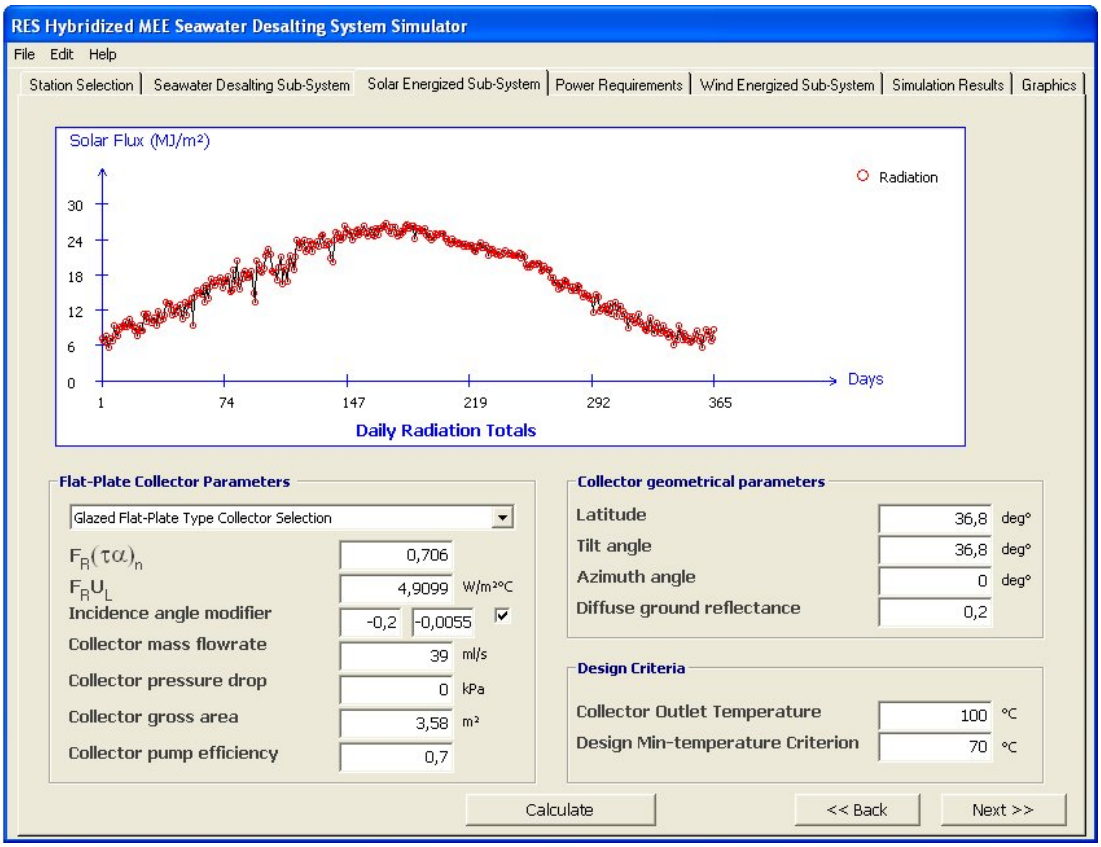

Figure 6.4 Design layout of solar energized sub-system tab

After selecting a collector type from the pull-down box and typing the other collector parameters, then clicking the “Calculate” button initiates the sub-program processing for each day of the year meeting the design criteria as seen in Fig. (6.5).

6.5 Power Requirements

Figure (6.6) shows the potential days over the x-axis maintaining the design min-temperature criterion and the daily power requirements during the system operation. Power needed by the vacuum system is taken from a manufacturer’s

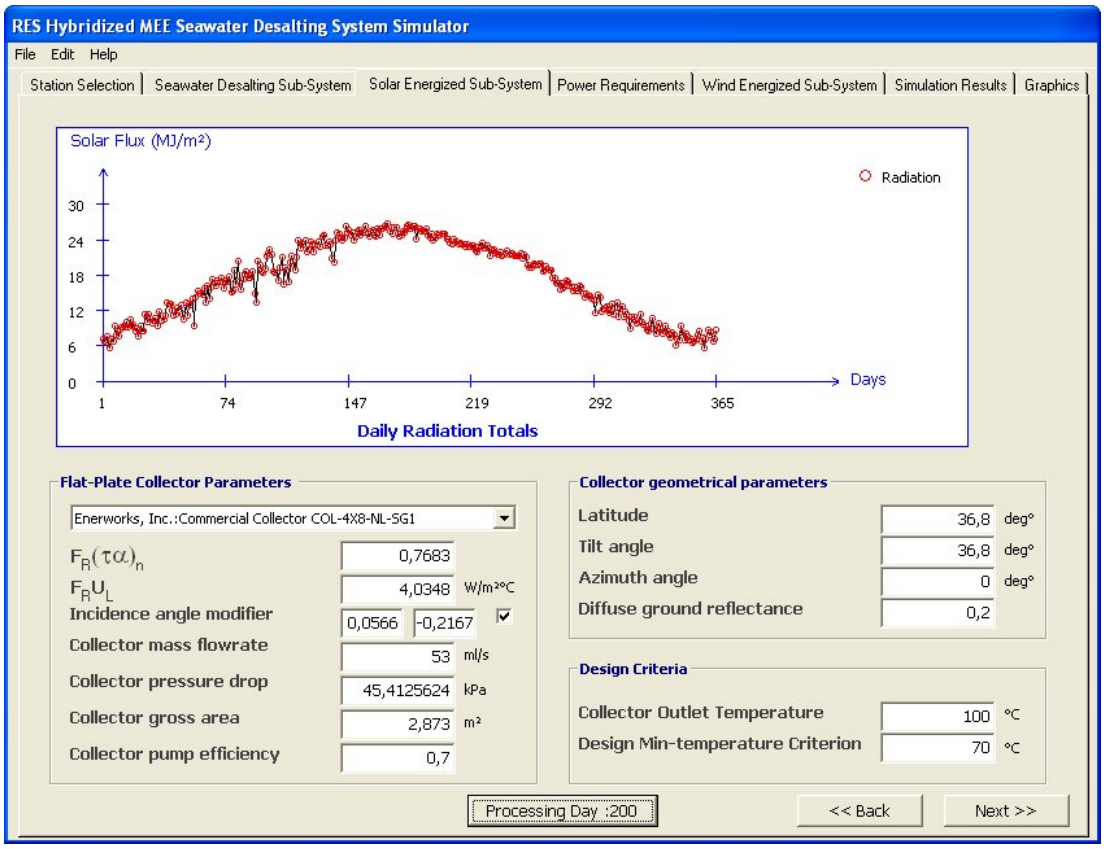

Figure 6.5 Selection of collector, assignment of design criteria and processing step

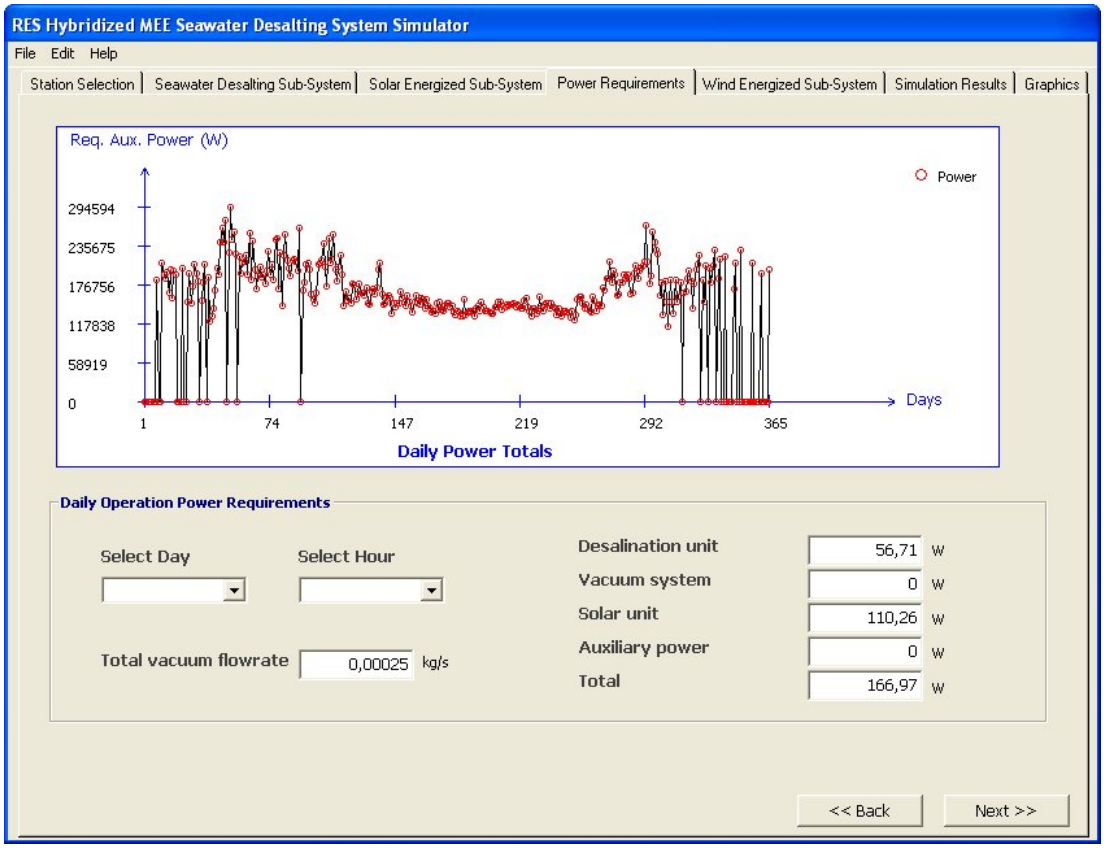

Figure 6.6 Design layout of power requirement tab

catalogue corresponding to the total vacuum flowrate. By selecting a day and an hour, the daily operation power requirements of the sub-systems are displayed as shown in Figure (6.7).

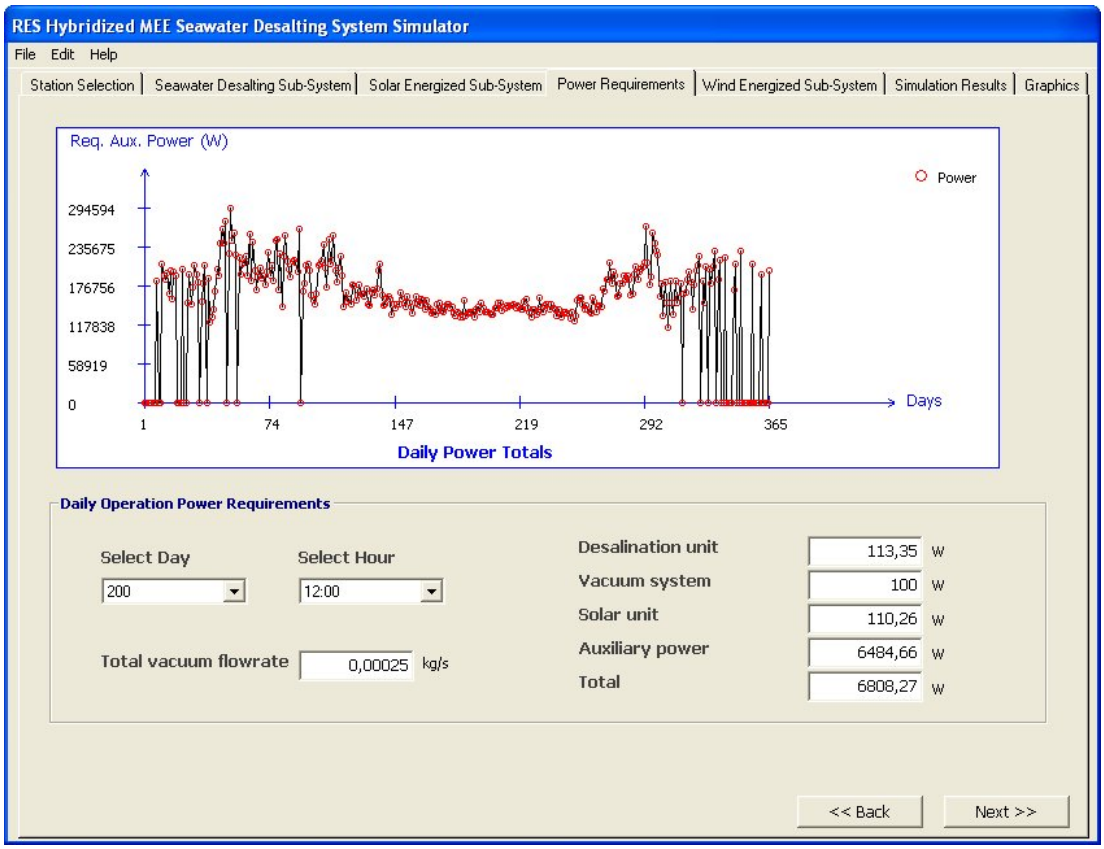

Figure 6.7 Power requirements for the selected day and hour

6.6 Wind Energized Sub-System

Figure (6.8) shows the average wind speeds over 24-hours with respect to the wind directions for the selected year. The selection of the year is determined to take into account the sum of the speeds over the corresponding year according to the wind directions. After the velocity summations are calculated for all years, they are summed up and divided into the number of year available. Correspondingly, the year is selected according to velocity summation result which is close to the average of the velocity summations of the available years.

It is deduced from the figure which direction has higher average speed. Based on this figure, wind turbine site should be decided to take into consideration the dis-

tribution of speed regarding to the directions.

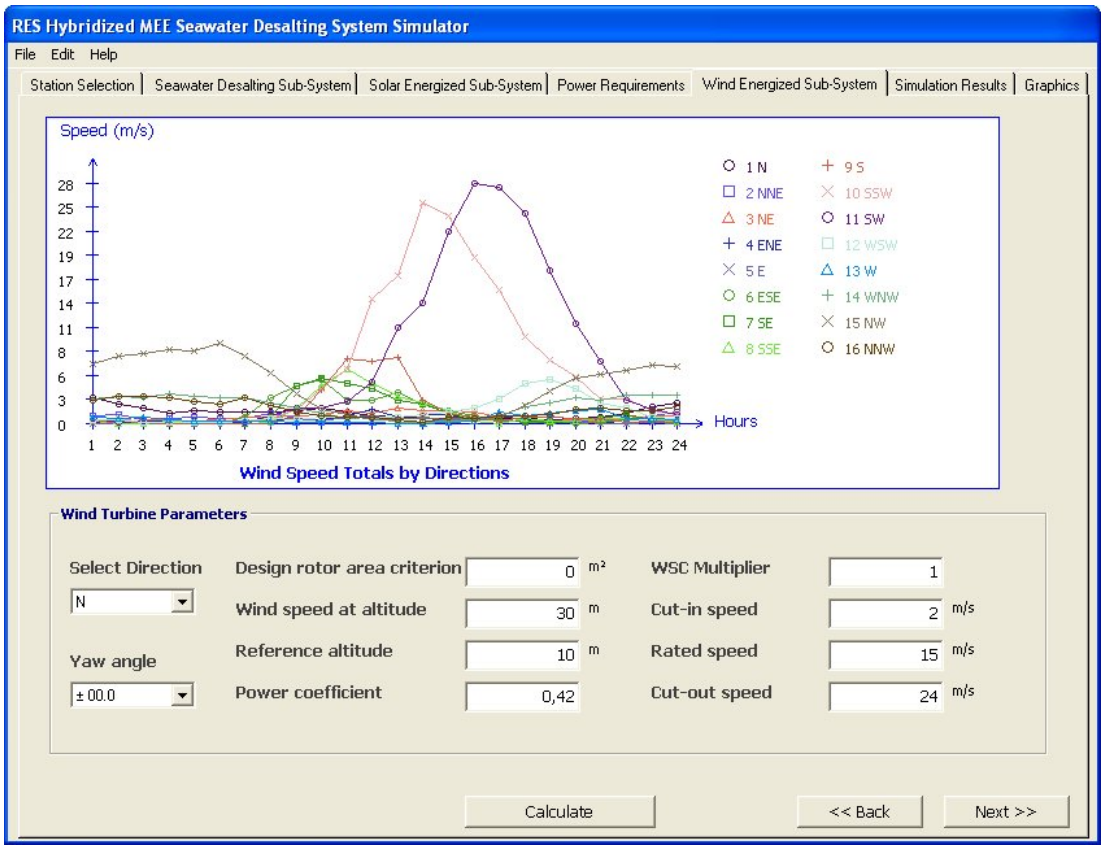

Figure 6.8 Design layout of wind energized sub-system tab

Wind turbine parameters are seen in Figure (6.8). Basic terminology regarding to wind turbine design can be expressed as below.

The **power coefficient** c_P expresses how efficiently a turbine converts the energy in the wind to electricity.

The shape of the calculated power curve is determined by three key elements relating power output to wind speed:

The **cut-in velocity** v_{CI} is the wind speed where the turbine starts to deliver power. In other words, the rotor must already be delivering enough power to compensate for the power loss in the drive train and to cover internal consumption.

The **rated wind velocity** υ_R is the wind speed at which the rated generator power is reached. It is identical with the permanently permissible maximum generator power output.

The **cut-out velocity** υ_{CO} is the highest wind speed at which the turbine may be operated while delivering power.

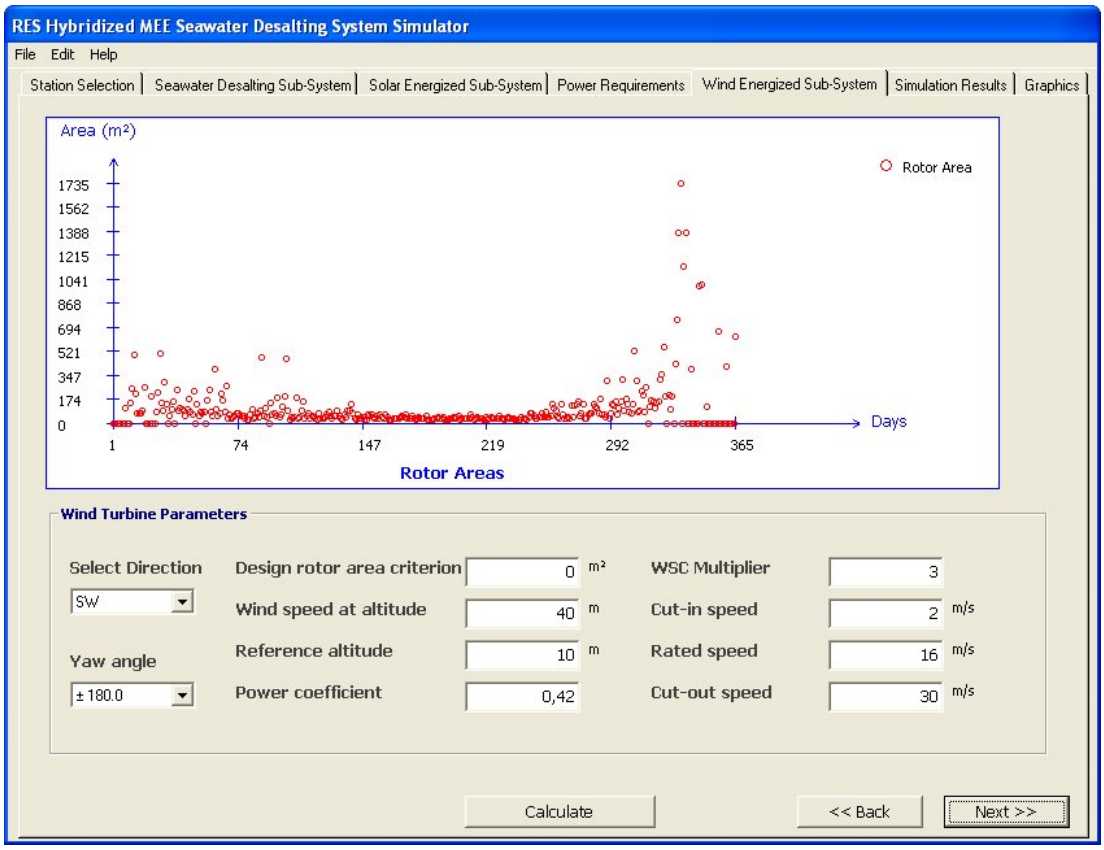

Figure 6.9 Assignment of wind turbine parameters and rotor area calculation step

After entering turbine parameters and then clicking the "Calculate" button, the required rotor areas for each day of the year are determined. Calculated results are exhibited in the Area vs. Days graphic in Figure (6.9). This graphic gives an idea about the distribution of area values and where they are cumulated mostly. Taking into consideration this graphic and turning back to the previous tab, according to the values of total power requirement which is to be met from a wind turbine whose rotor area can be taken from a manufacturers' catalogue, design rotor area criterion text-box can be set in accord with these relations. Design rotor area criterion defines

the potential days, with respect to the areas remaining under the criterion value, from the aspect of wind energy availability as shown in Figure (6.10).

The total working potential day is determined according to two criteria. One of them is the design min-temperature criterion and the other one is the design rotor area criterion. These criteria depend on each other but the determination of the total potential day is initiated with the design min-temperature criterion at first. The remaining days left from the previous criterion are subjected to the second criterion and eventually the total potential days are determined.

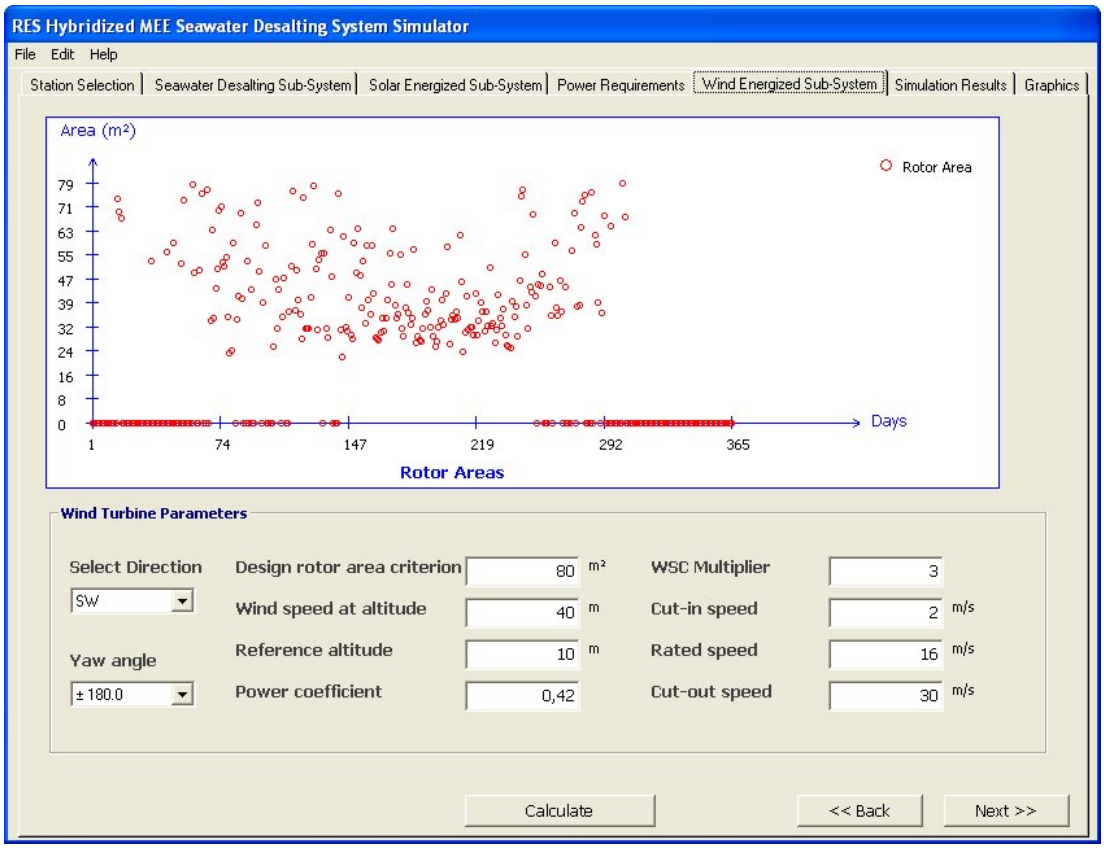

Figure 6.10 Design rotor area criterion result

6.7 Simulation Results

After the design parameters of overall system are assigned, the system results can be seen under the "System Result" tab. It is easily viewed the simulation results of the sub-systems on the MSFlexGrid control, clicking on the picture box as seen in Figure (6.11).

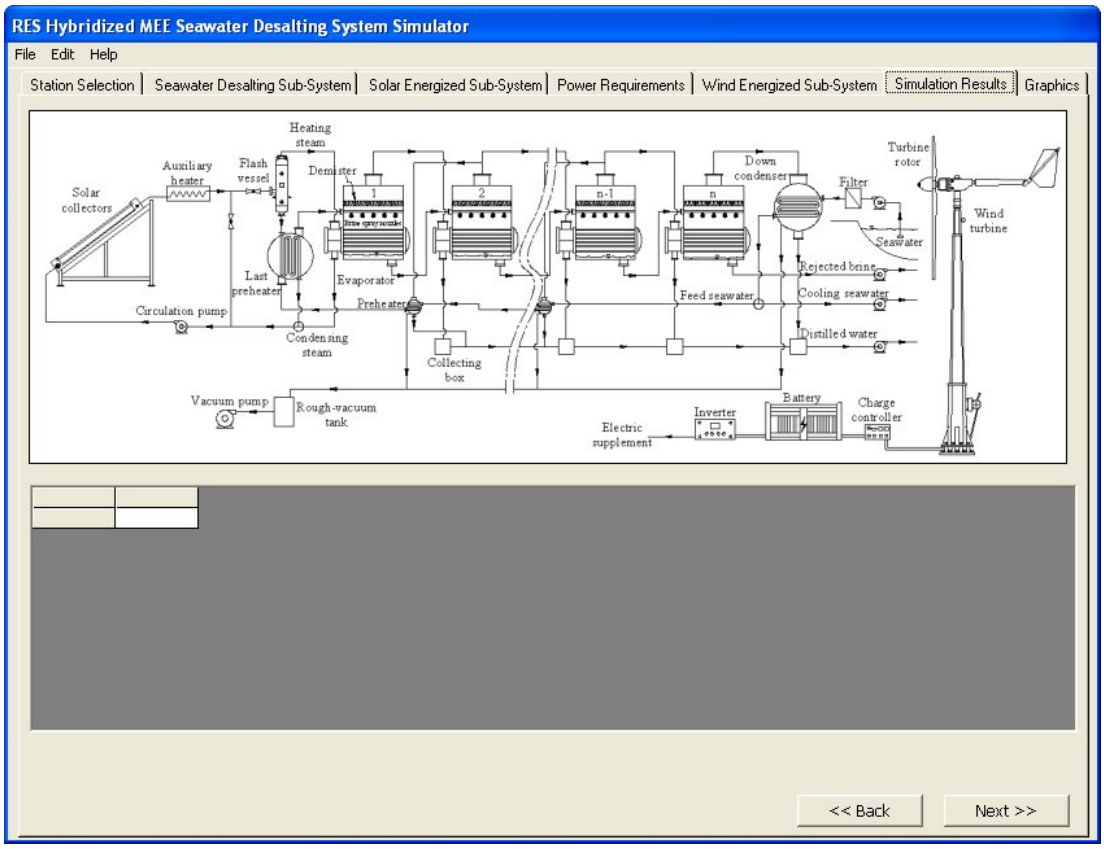

Figure 6.11 Design layout of system results tab

Figure (6.12) displays the effect results and it includes effect temperatures, saturated pressure in the effects, vapor saturation temperature, boiling point elevation, flashing temperature, non-equilibrium allowance, condensation temperature, bundle losses, evaporated vapor mass flowrate, flashed off vapor mass flowrate, brine mass flowrate, brine salt concentration, evaporator area, evaporator overall heat transfer coefficient, respectively.

Figure (6.13) displays the preheater results and it includes the inlet and outlet temperatures of feedwater from preheaters, flashing temperature, flashing condensation temperature, feedwater mass flowrate, flashing steam mass flowrate and preheater area, respectively.

The results regarding to down condenser are shown in Figure (6.14) which includes cooling seawater temperature, feed seawater temperature, vapor saturation temperature, condensation temperature, condenser area and overall heat transfer coefficient, respectively.

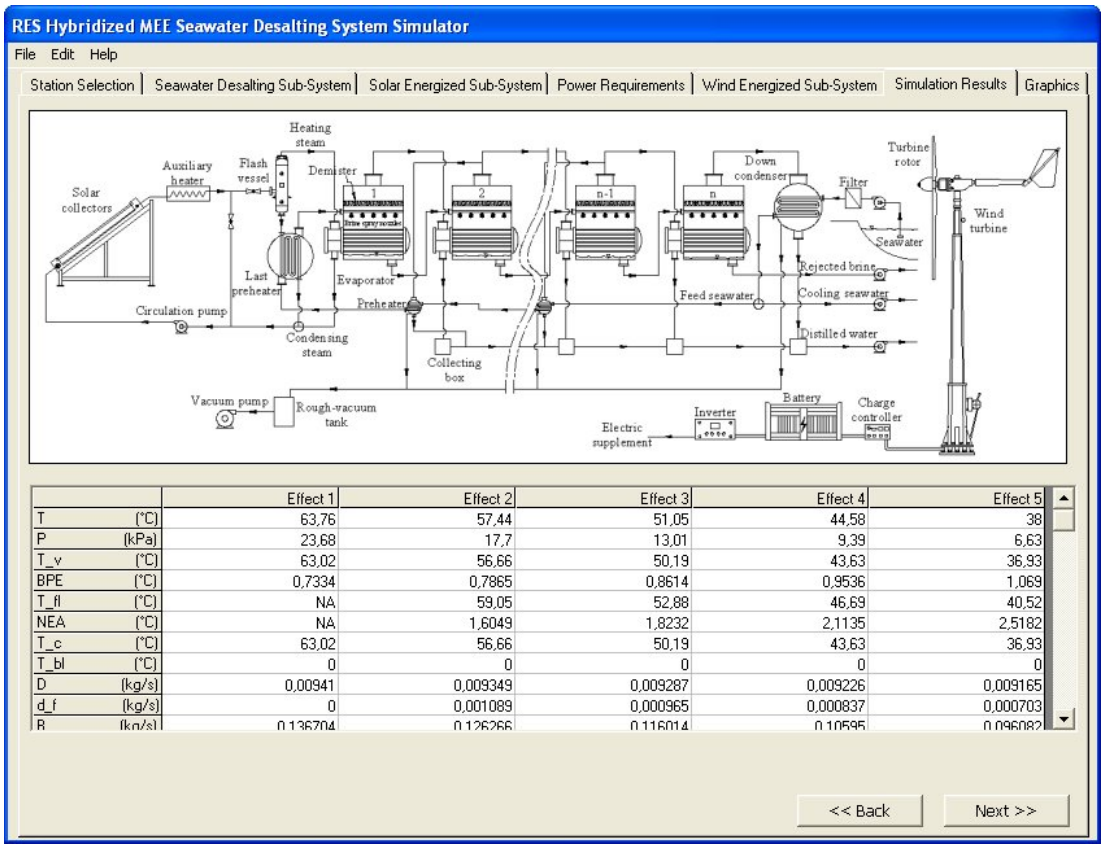

		Effect 1	Effect 2	Effect 3	Effect 4	Effect 5
T	(°C)	63,76	57,44	51,05	44,58	38
P	(kPa)	23,68	17,7	13,01	9,39	6,63
T_v	(°C)	63,02	56,66	50,19	43,63	36,93
BPE	(°C)	0,7334	0,7865	0,8614	0,9536	1,069
T_fl	(°C)	NA	59,05	52,88	46,69	40,52
NEA	(°C)	NA	1,6049	1,8232	2,1135	2,5182
T_c	(°C)	63,02	56,66	50,19	43,63	36,93
T_bl	(°C)	0	0	0	0	0
D	(kg/s)	0,00941	0,009349	0,009287	0,009226	0,009165
d_f	(kg/s)	0	0,001089	0,000965	0,000837	0,000703
B	(kg/s)	0,136704	0,126266	0,116014	0,10595	0,096082

Figure 6.12 Effect results of MEE-FF seawater desalination sub-system

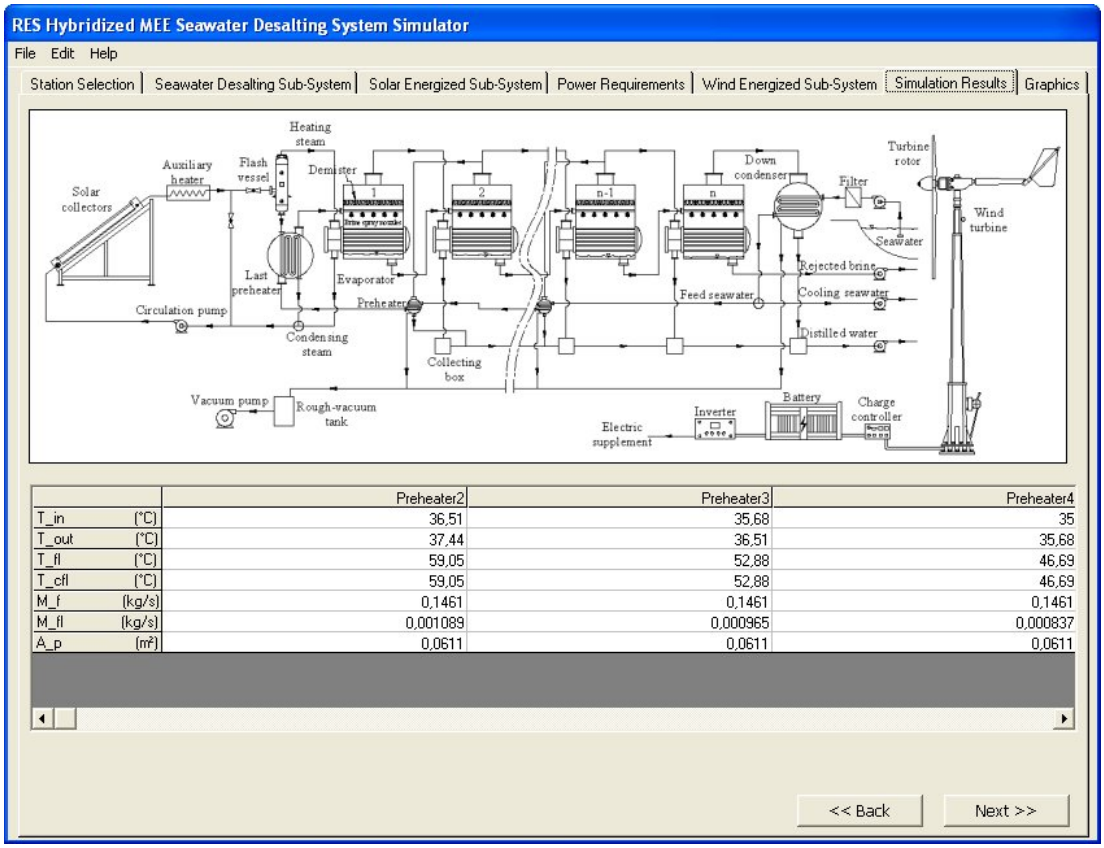

		Preheater2	Preheater3	Preheater4
T_in	(°C)	36,51	35,68	35
T_out	(°C)	37,44	36,51	35,68
T_fl	(°C)	59,05	52,88	46,69
T_cfl	(°C)	59,05	52,88	46,69
M_f	(kg/s)	0,1461	0,1461	0,1461
M_fl	(kg/s)	0,001089	0,000965	0,000837
A_p	(m²)	0,0611	0,0611	0,0611

Figure 6.13 Preheater simulation results

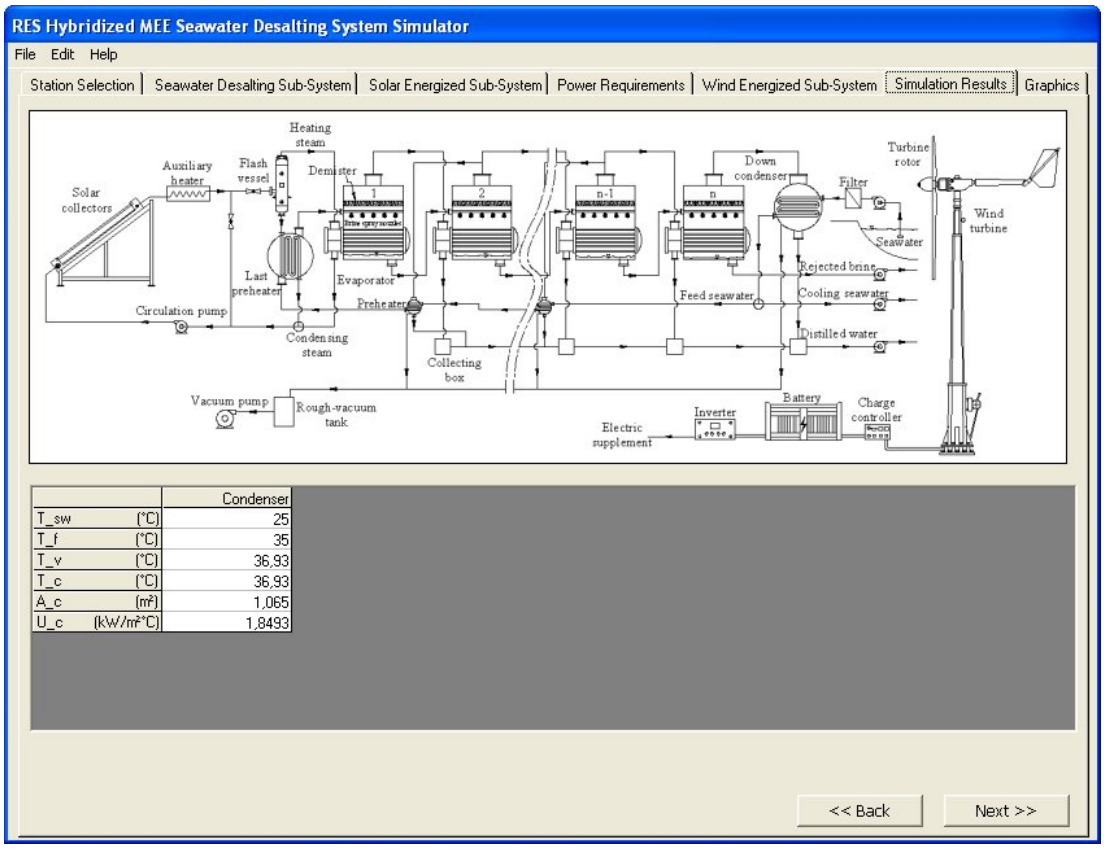

Figure 6.14 Down condenser simulation results

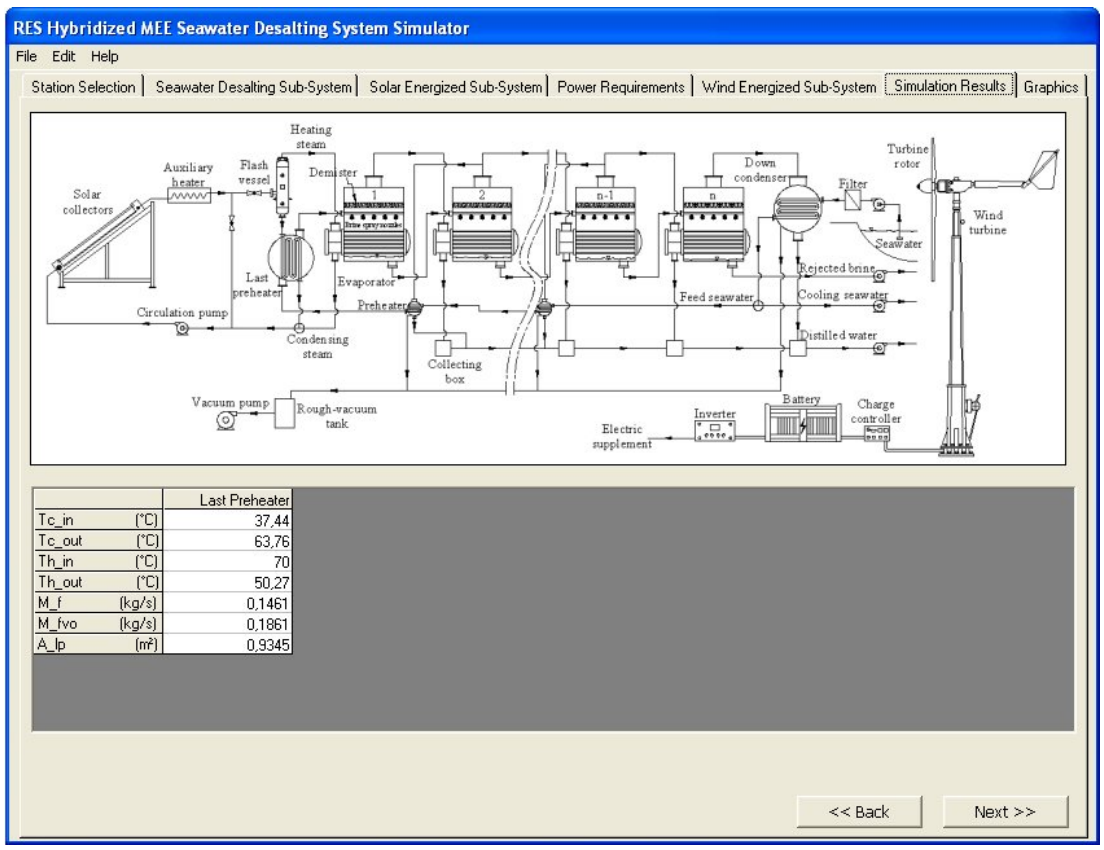

Figure 6.15 Last preheater simulation results

Figure (6.15) represents the results of last preheater which are put in order as cold fluid inlet and outlet temperatures, hot fluid inlet and outlet temperatures, feed seawater (heated fluid) mass flowrate, flash vessel condensate (cooled fluid) mass flowrate and last preheater area, respectively.

Figure (6.16) illustrates the amount of mass flowrates regarding to the seawater desalination sub-system. In order to see the simulation result, the selection of the operation day must be made initially. The results include feed seawater mass flowrate, cooling seawater mass flowrate, feed seawater mass flowrate, rejected brine mass flowrate, distillate water mass flowrate, and the daily distillate production, respectively.

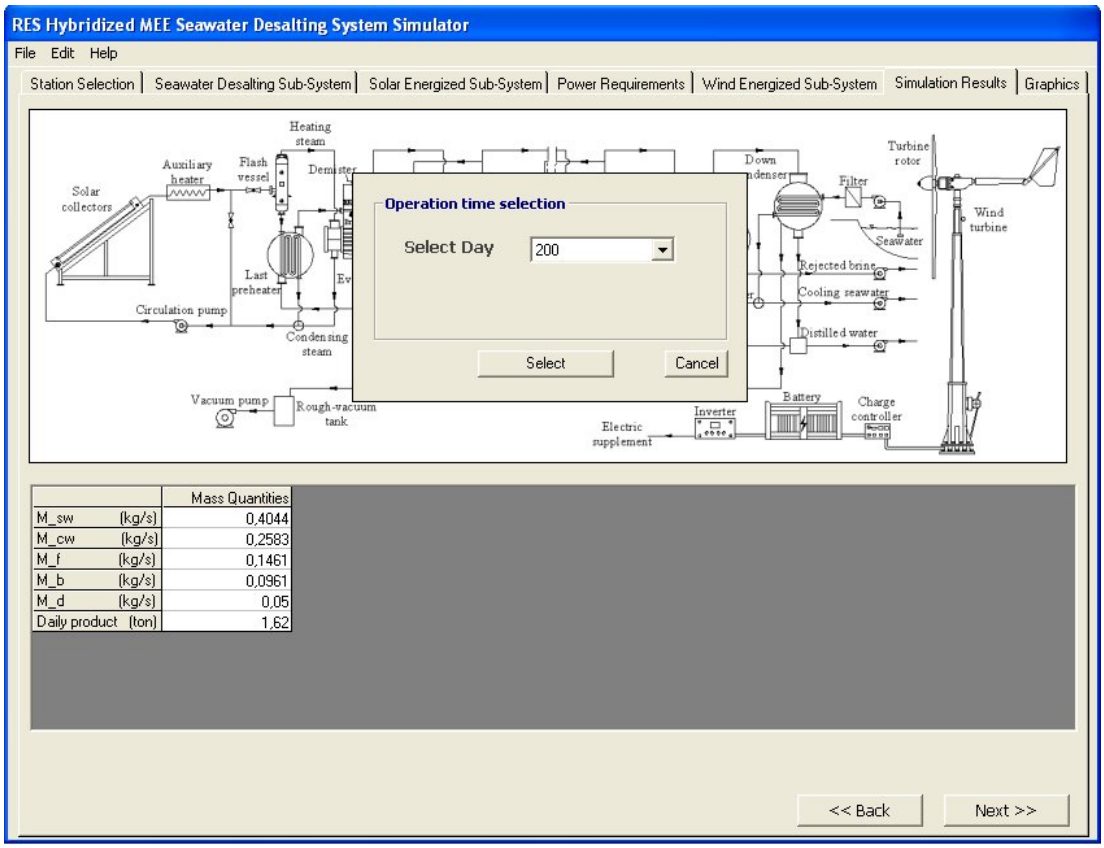

Figure 6.16 Mass balance simulation results

Figure (6.17) exhibits the simulation results of flash vessel which are inlet temperature of the working fluid to flash vessel and the corresponding saturated pressure, condensate temperature in the flash vessel and the corresponding saturated

pressure, steam temperature, mass flowrate entering flash vessel, condensate mass flowrate outgoing from flash vessel, mass flowrate of steam generated, respectively.

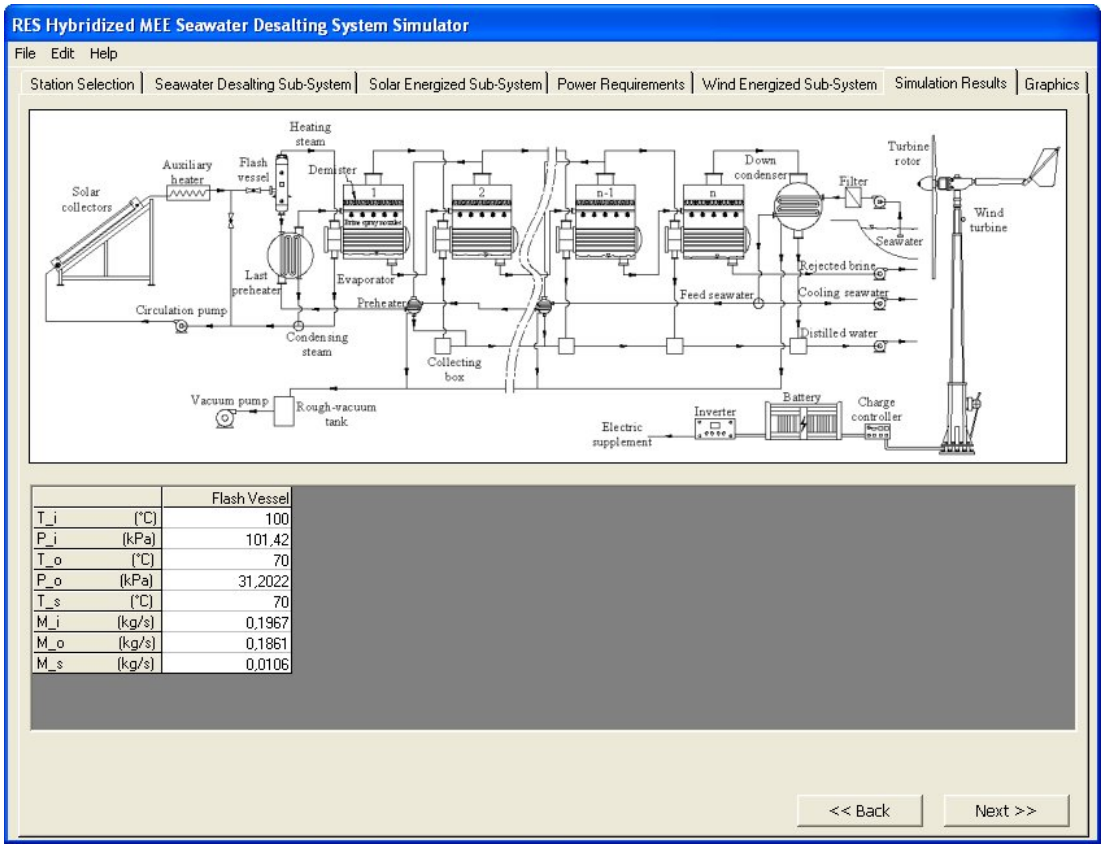

Figure 6.17 Flash vessel simulation results

Figure (6.18) shows the results regarding to the closed-loop solar collector system. Operation time selection is required because the solar flux data are hourly-changing within the days of the year. After the selection is made, the collector fluid inlet and outlet temperatures for the series, the efficiencies of the collector series, pressure at the collector pump inlet, pressure at the collector pump outlet, pressure drop across the inlet and outlet of the series collector, number of collector connected series, number of collector connected parallel and the total required collector area can be viewed from the chart.

Figure (6.19) shows the values of the power must be met from the wind turbine during the system operation for the selected day.

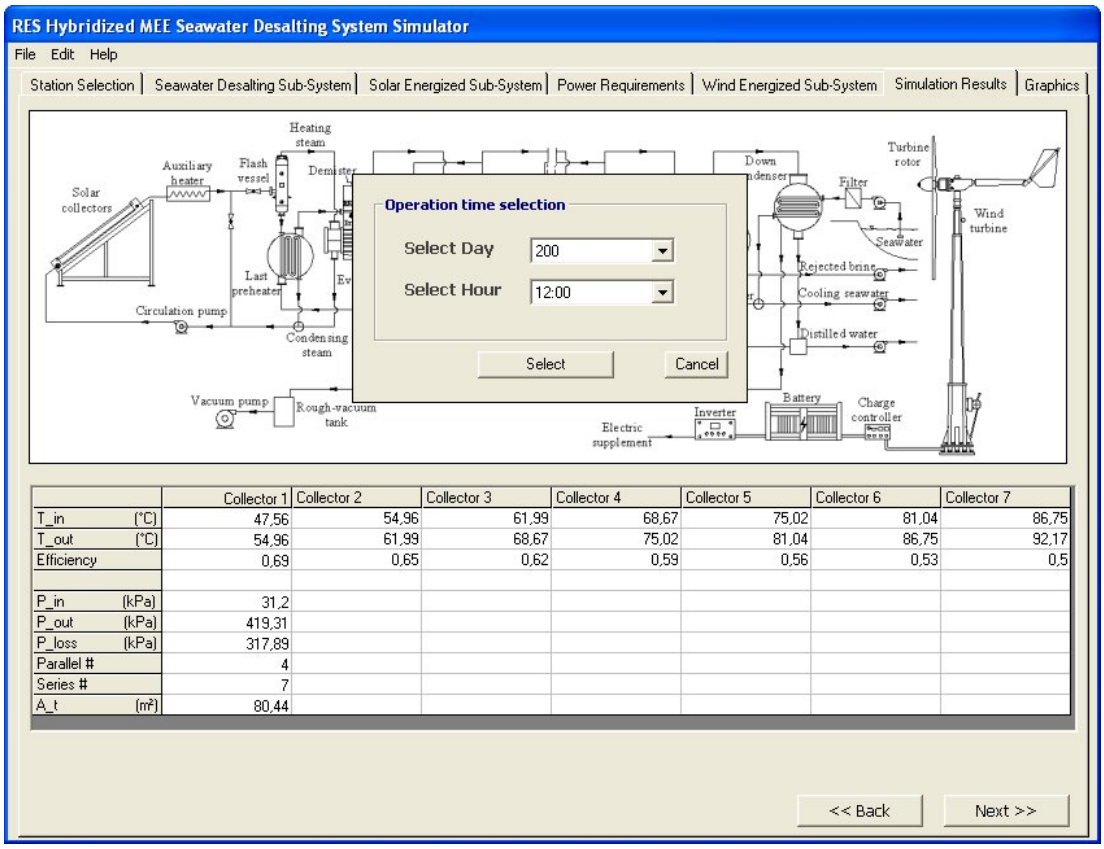

Figure 6.18 Flat-plate solar collector simulation results

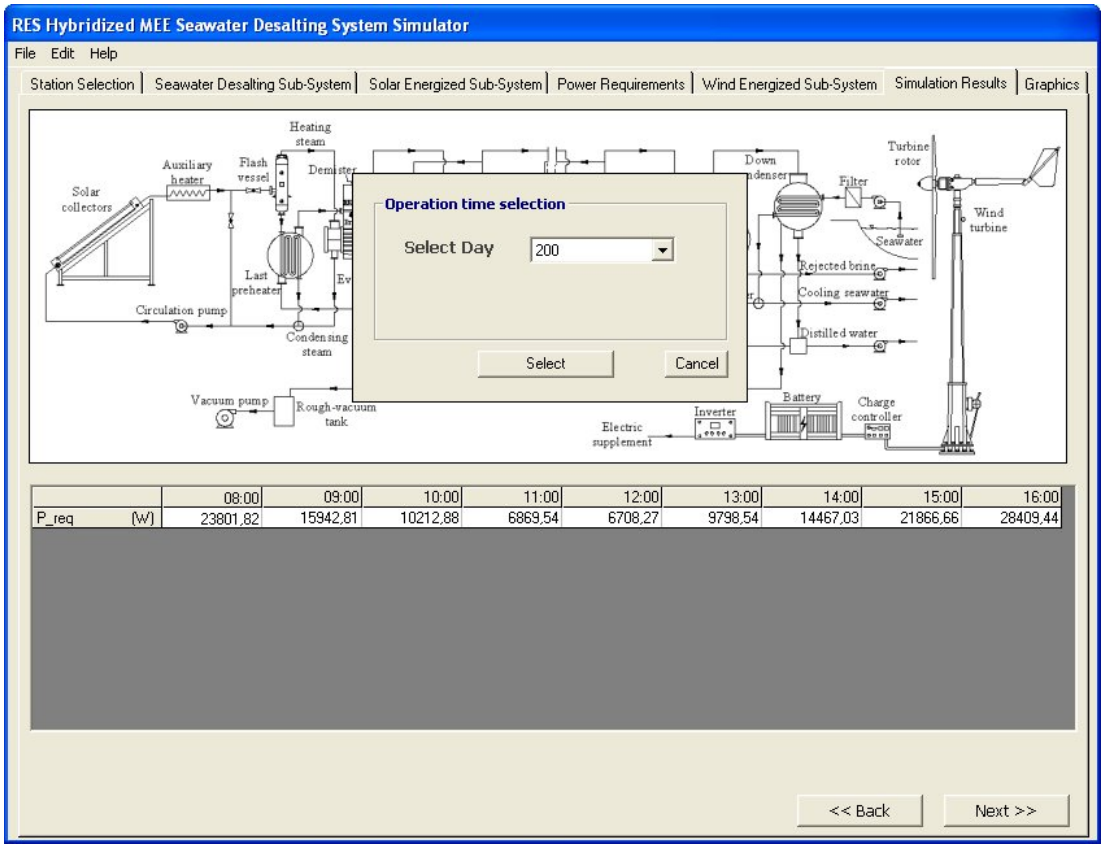

Figure 6.19 Wind turbine simulation results

6.8 Simulation Graphics

In this section, the validity of the developed models with the literature studies will be demonstrated on behalf of the sub-systems. After the models approaches are provided acting from this point, the feasibility study on the selection of suitable station is to be achieved under the light of these knowledge.

The developed model for seawater MEE desalination system is to be validated from the aspects of the effects, preheaters analysis and also system performance characteristics.

Figure (6.20) represents the temperature profiles of the feed seawater through the preheaters and the effects.

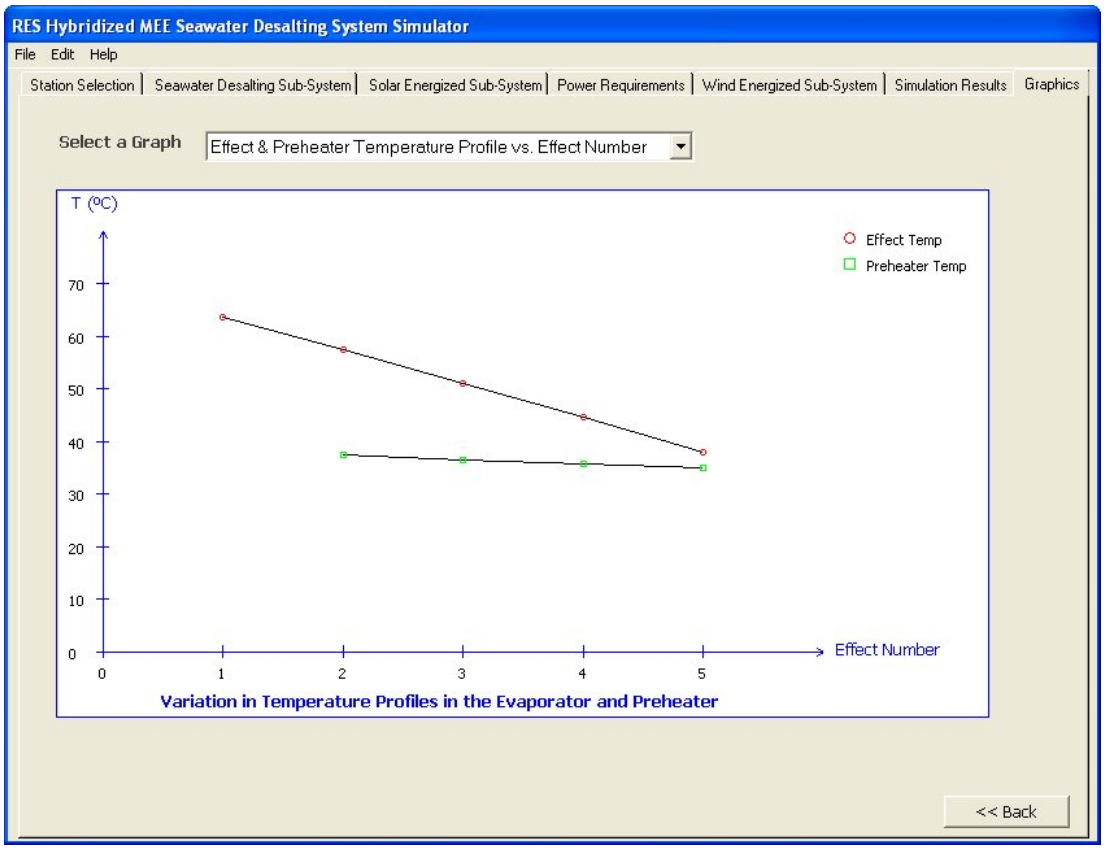

Figure 6.20 Variation in temperature profiles in the evaporator and preheater

Figure (6.21) shows the distillate flowrates leaving each effect generated by boiling and flashing processes. It is understood from the figure, the major part of the

total distillate is formed by boiling whose rate decreases in subsequent effects due to smaller latent heat of vaporization at lower temperature. The amount of distillate formed by flashing inside each effect is negligible compared with the boiled. Notwithstanding the flashing vapors are used to increase the feed seawater from 35°C to a higher temperature. And then it is heated by the last preheater up to the top brine temperature.

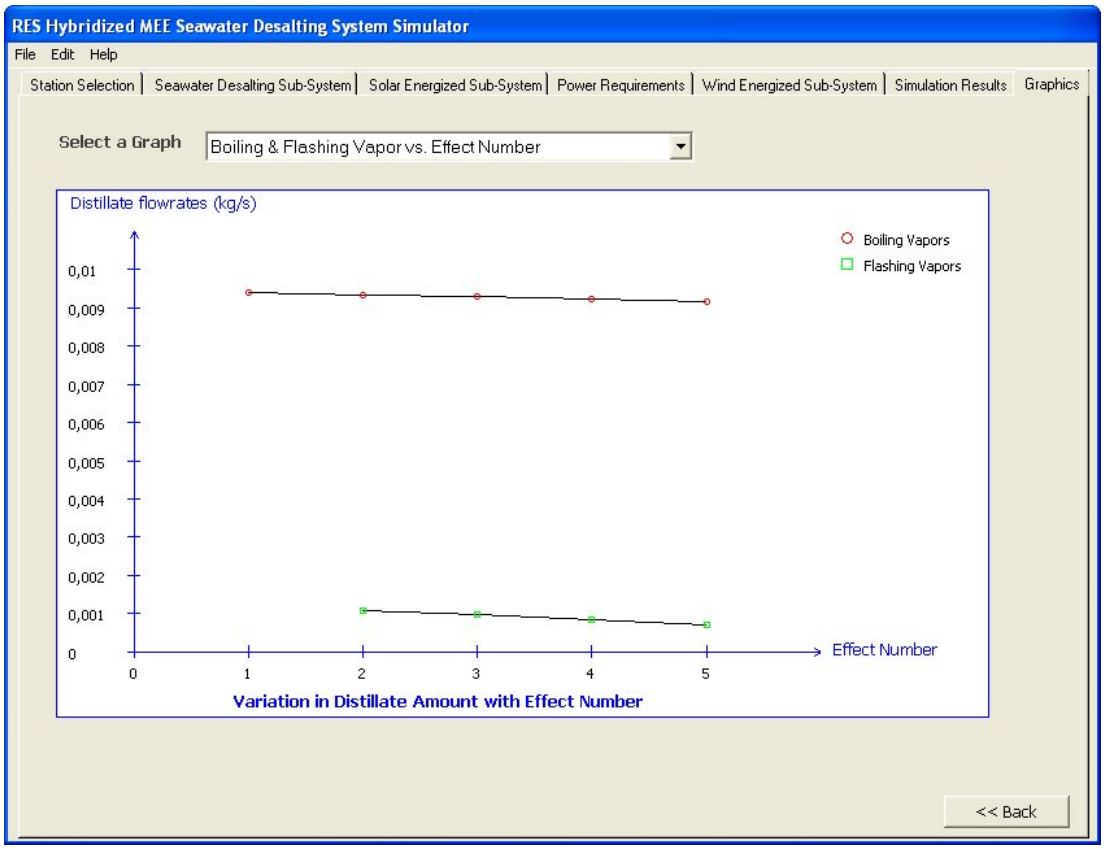

Figure 6.21 Variation in distillate amount with effect number

The analysis regarding to the system performance parameters graphics are based on the following definitions.

Performance ratio PR, which is defined as the amount of the distillate product per unit mass of the heating steam.

$$PR = \frac{\dot{m}_d}{\dot{m}_s} \tag{6.1}$$

Specific heat transfer area $s(A)$, which is defined as the ratio of the total heat transfer area of the evaporator and condenser to the total flow rate of distillate product.

$$s(A) = \frac{\left(\sum_{i=1}^{n} A_e + A_c \right)}{\dot{m}_d} \tag{6.2}$$

Specific flow rate of cooling water $s(\dot{m}_{cw})$, which is defined as the amount of the cooling water per unit mass of distillate product.

$$s(\dot{m}_{cw}) = \frac{\dot{m}_{cw}}{\dot{m}_d} \tag{6.3}$$

Conversion ratio CR, which is defined as the amount of distillate product per unit mass of feed seawater.

$$CR = \frac{\dot{m}_d}{\dot{m}_f} \tag{6.4}$$

Figure (6.22) illustrates the effect of the number of effects on the performance ratio for different top brine temperatures. It is seen that the performance ratio increases when the number of effects increases. Thus, the increase in the number of effects increases the distillate production for almost the same amount of heating steam. The developed mathematical model of the MEE sub-system is in accordance with the reference [2] when they are considered. On account of the fact that the model assumptions show some differences with the literature, the performance graphic may exhibit small distinctions still the results are consistent with the literature.

Figure (6.23) illustrates the variation on the specific heat transfer area by varying TBT and the number of effects. It is seen that the specific heat transfer area increases at lower TBT and higher number of effects.Using higher number of effects

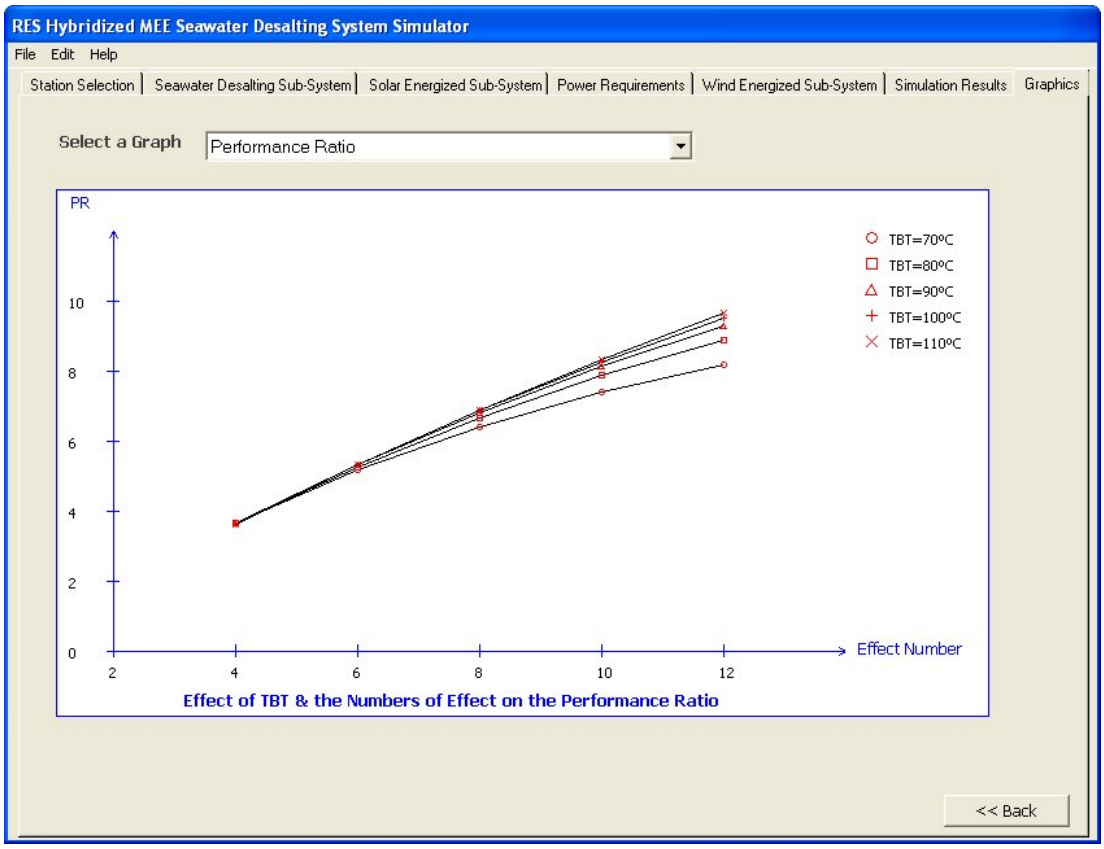

Figure 6.22 Effect of TBT & the numbers of effect on the performance ratio

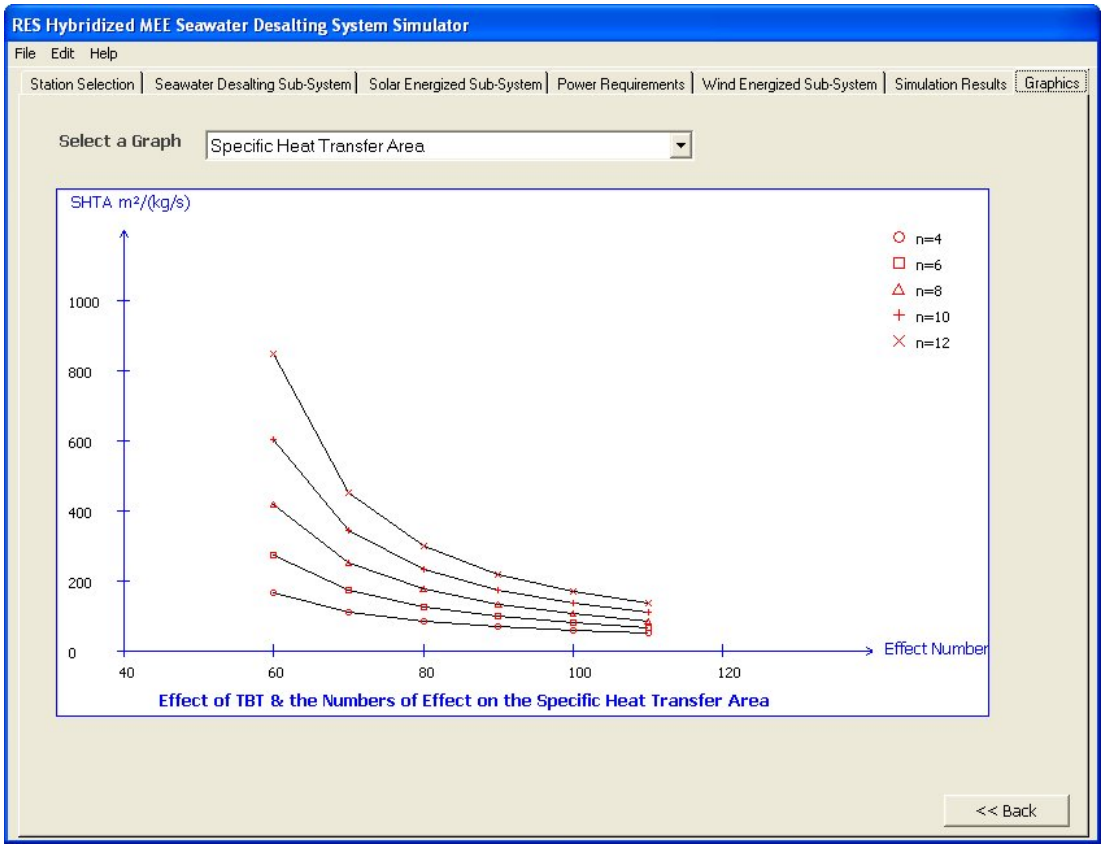

Figure 6.23 Effect of TBT & the numbers of effect on the SHTA

decreases the temperature difference between the effects and the overall heat transfer coefficients. Therefore, keeping the top brine temperature constant and increasing the number of effects gives rise to the increase of the specific heat transfer area. The obtained graphic shows satisfactory agreement between the model and the referenced model [1].

It is understood from the Fig. (6.24), the variation in the conversion ratio is constant and independent from the TBTs. The graphic is drawn for three different intake seawater salinity concentrations regarding to the seas surrounding Turkey. Keeping the rejecting brine salinity concentration is constant and increase the intake seawater salinity concentration decreases the conversion ratio.

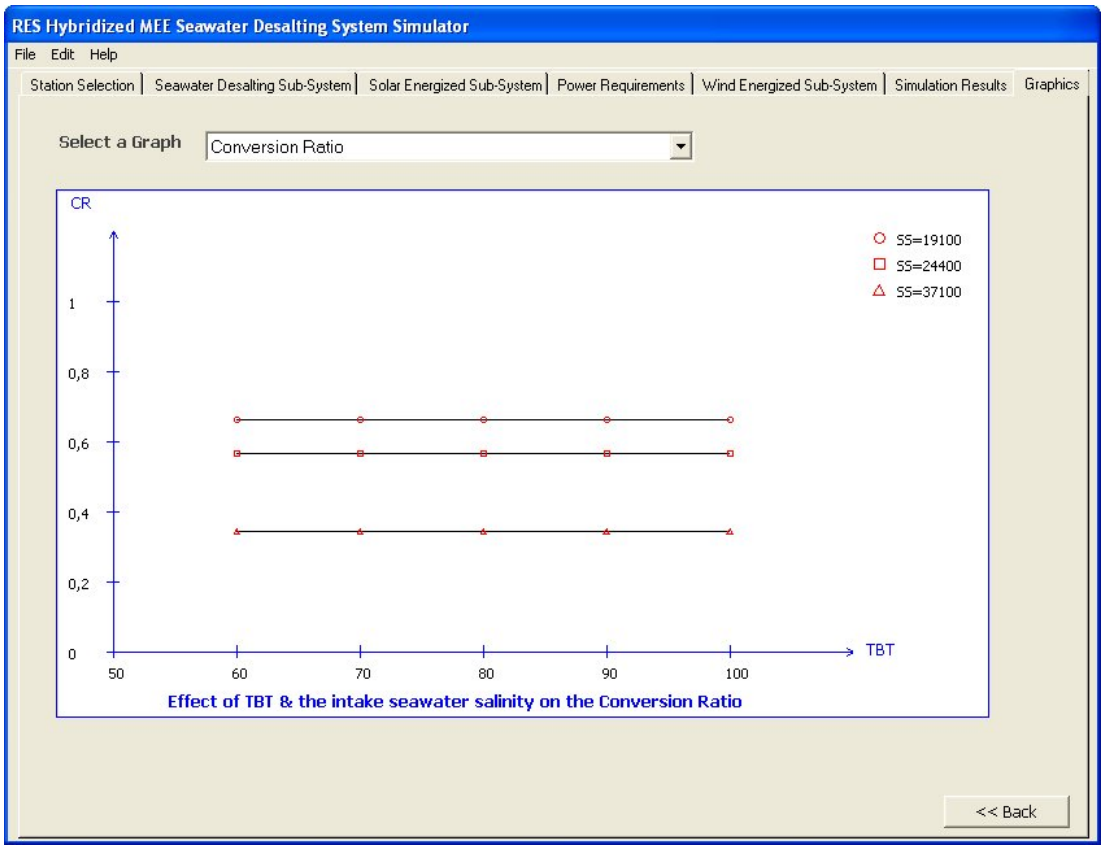

Figure 6.24 Effect of TBT & the intake seawater salinity on the conversion ratio

Figure (6.25) illustrates the variation on the specific cooling water flowrate by varying TBT and the number of effects. It is seen that the variation in the specific cooling water flowrate is nearly independent from TBT. On the other hand, the specific cooling water flowrate decreases rapidly with the increase in the number of

effects. Increasing the number of effects increases the total amount of distillate and reduces the amount of distillate formed in each effect thus the amount of cooling seawater needed for the down condenser decreases. The consistency of the obtained graphic can be seen from the reference [15]. However, there may have small differences between the obtained results and the reference due to some distinctions in the composed system models.

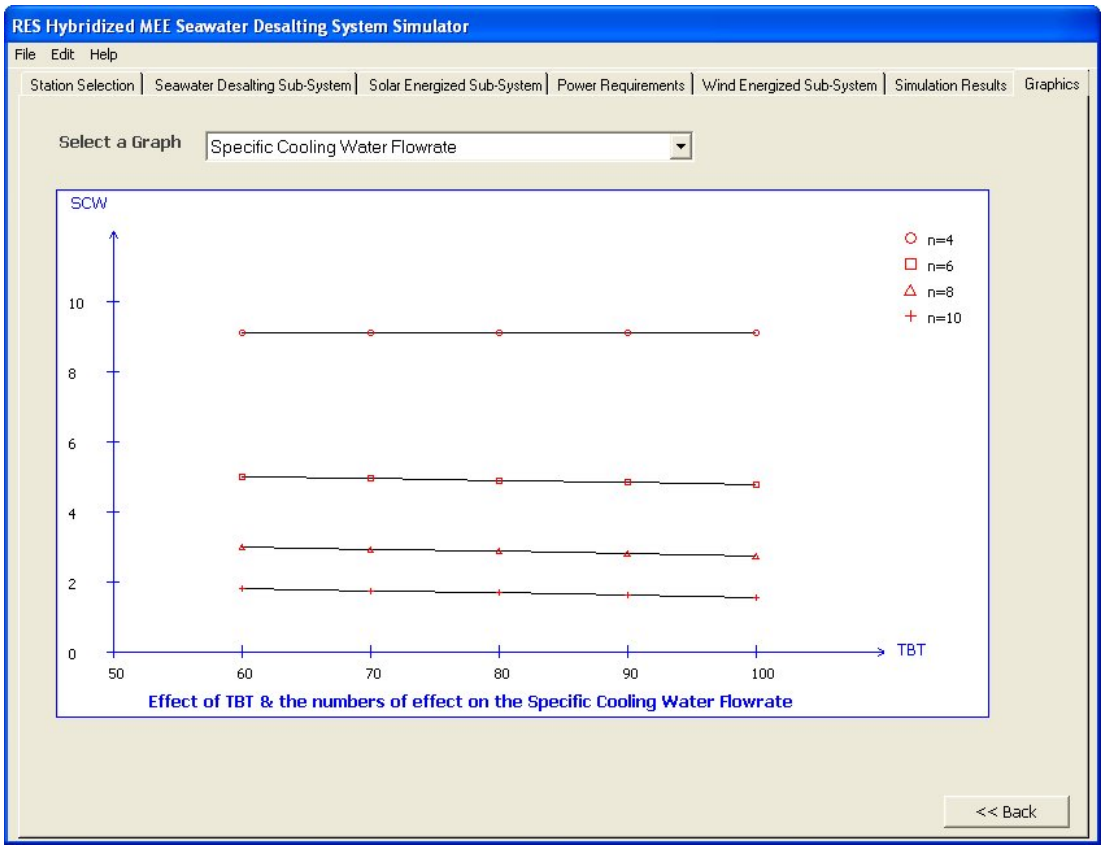

Figure 6.25 Effect of TBT & the numbers of effect on the SCWF

Figure (6.26) shows the variation in the cooling seawater mass flowrate through the year. Design area of condenser was determined considering a fixed seawater temperature at the condenser inlet and feed seawater temperature at the condenser outlet. Correspondingly, variation in the inlet seawater temperature on a certain day varies the mass flowrate entering the condenser due to having a constant heat transfer area. As it seen from the figure, cooling seawater mass flowrate increases during the summer because of having higher seawater temperature in this period.

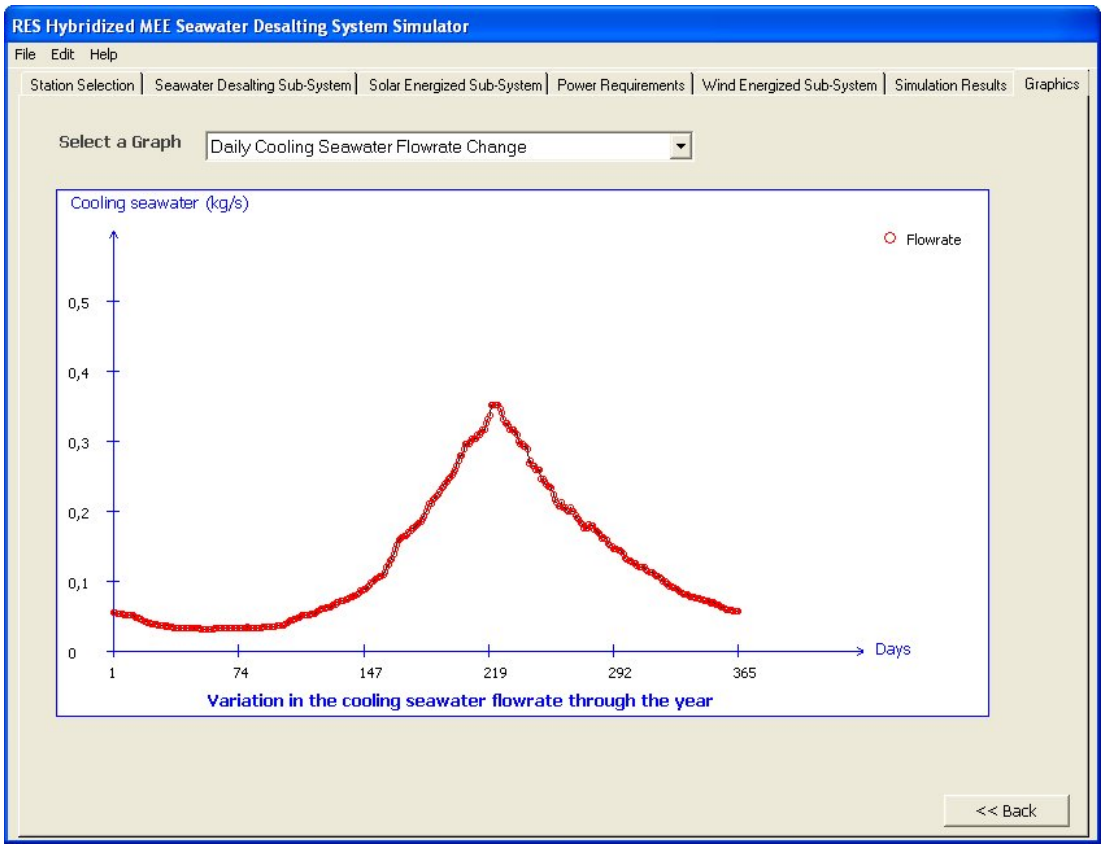

Figure 6.26 Variation in the cooling seawater mass flowrate through the year

Figure (6.27) exhibits the change in temperature profile through the collector series. The outlet temperature of the series goes up incrementally beginning from the first collector to end collector in the direction of positive slope as seen from the figure.

Figure (6.28) displays the thermal performance of collectors in the array that are connected series. It is seen from the figure, the slope of the graph will decrease as long as the number of collector in the series increases. Due to the fact that inlet temperature of the collector increases, the thermal efficiency of the collector decreases as it is understood from the Equation (4.14).

Figure (6.29) exhibits the working hours of the system during the potential days from the solar and wind energy availability point of view. The number of potential days from the aspect of renewable energy sources can be seen on the right-side of the graphic panel of the program. The solar energized sub-system working hours change with the seasonal period according to up-and-down variation in the

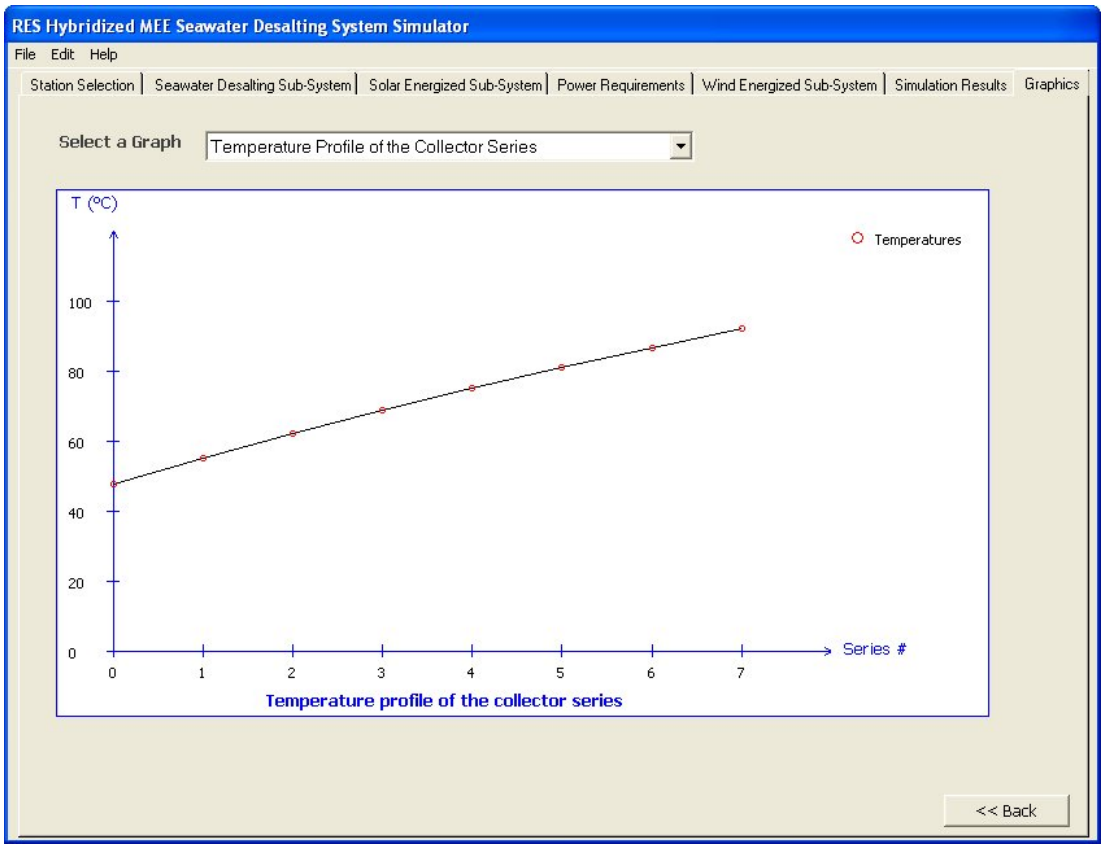

Figure 6.27 Temperature profile of the collector series

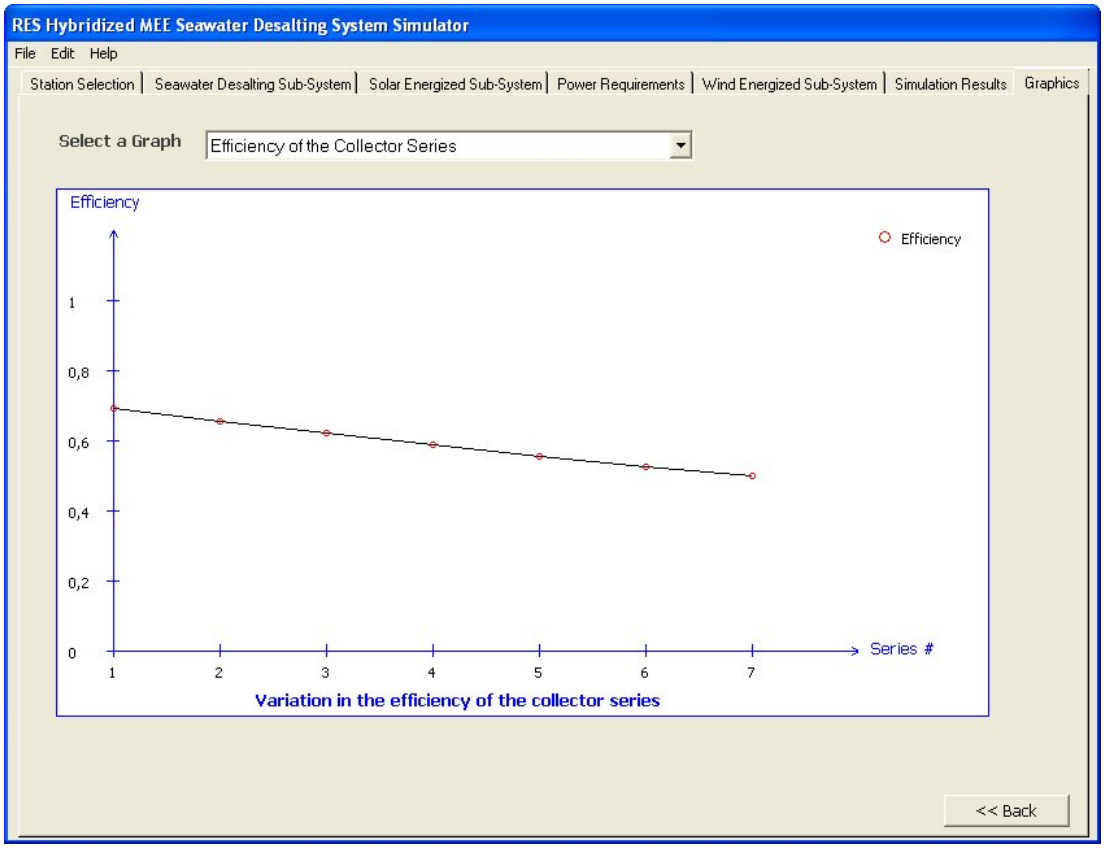

Figure 6.28 Variation in the efficiency of the collector series

solar flux. On the other hand, the wind turbine working hour changes with changing in the wind speed value remaining under the cut-in speed.

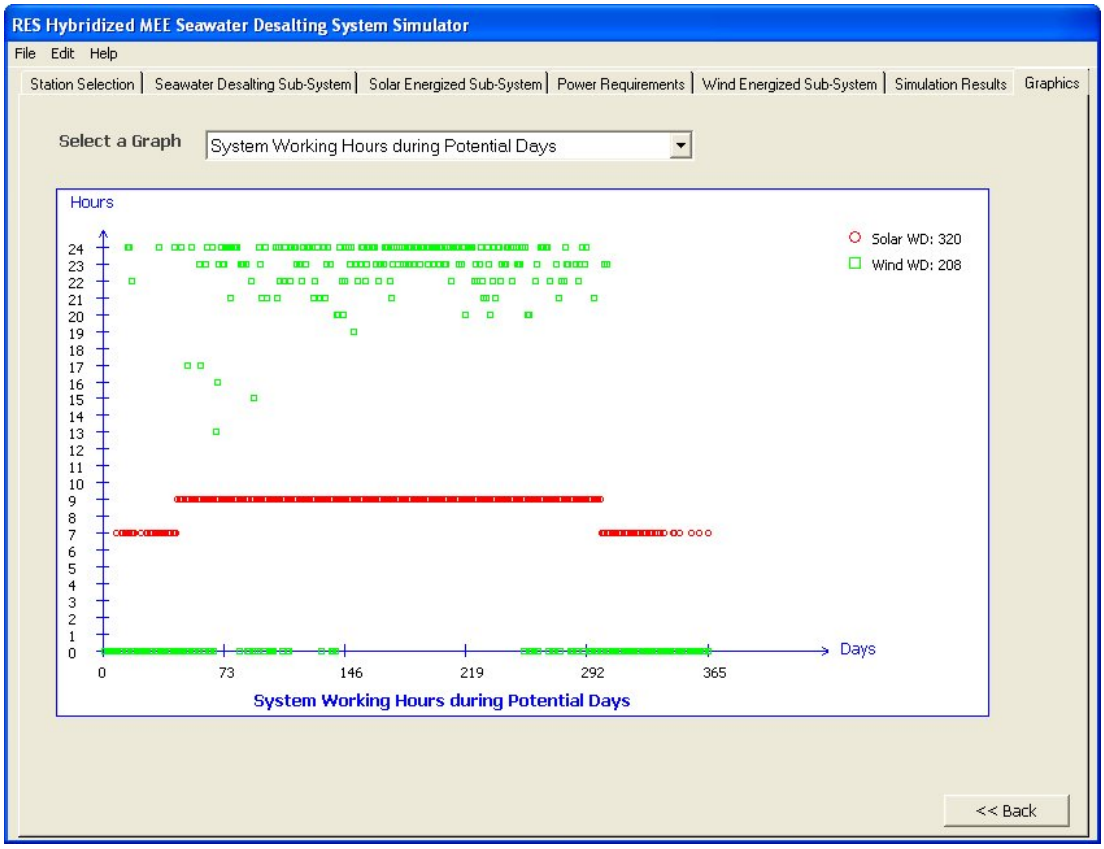

Figure 6.29 Total system working hours during the potential days

Figure (6.30) shows the electrical demand and supply profiles of the sub-systems and wind turbine, respectively. These two profiles refer to the typical power demand of the sub-systems and the power produced by wind turbine for the selected day of the year. The power requirement of the system decreases in the mid-hours of the day due to higher solar fluxes as seen from the figure. Wind power amount can change during the day due to variation in the wind speeds.

Figure (6.31) displays the required collector areas for realizing the system design up to the solar energized sub-system tab. The sub-program makes the necessary calculations for each station keeping the result in the memory and finally sketches them onto the graphic panel. Making these calculations for identical sub-systems, all of the sub-system parameters are kept constant except the parameters such as intake seawater salinity, latitude, tilt angle etc. belongs to the corresponding

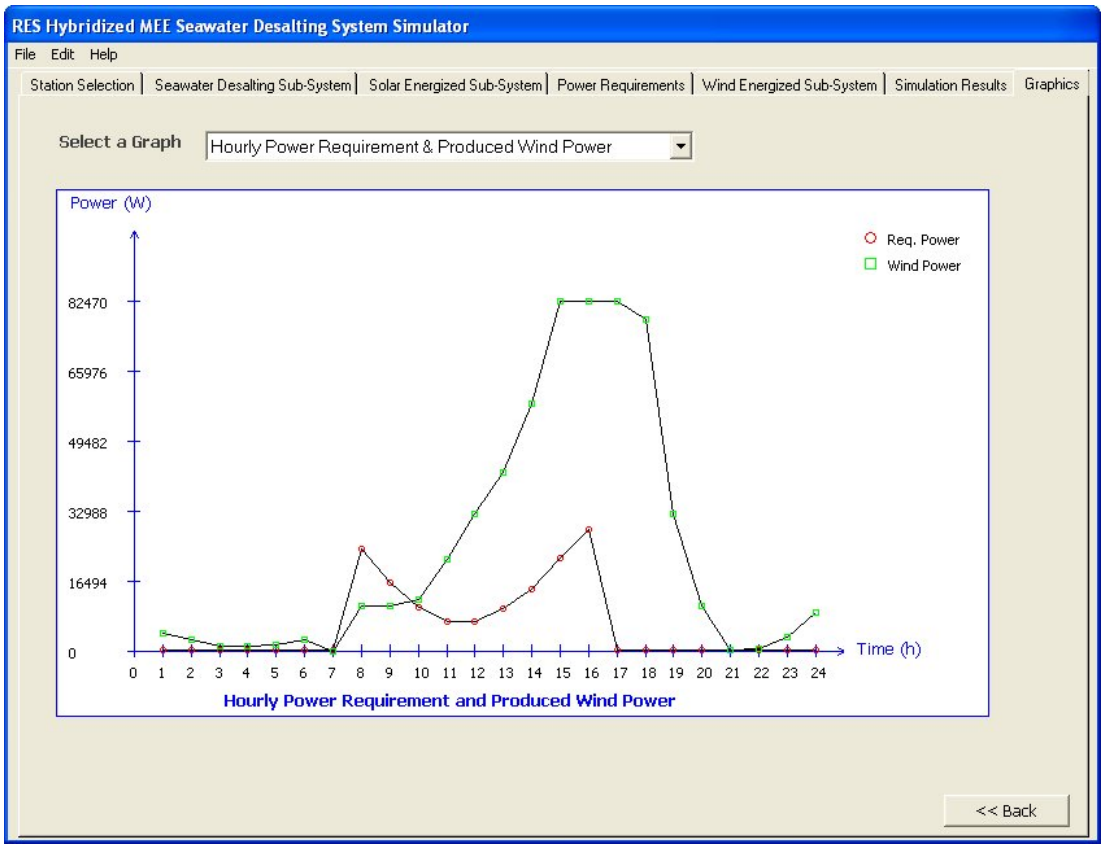

Figure 6.30 Hourly power requirement of the system and produced wind power

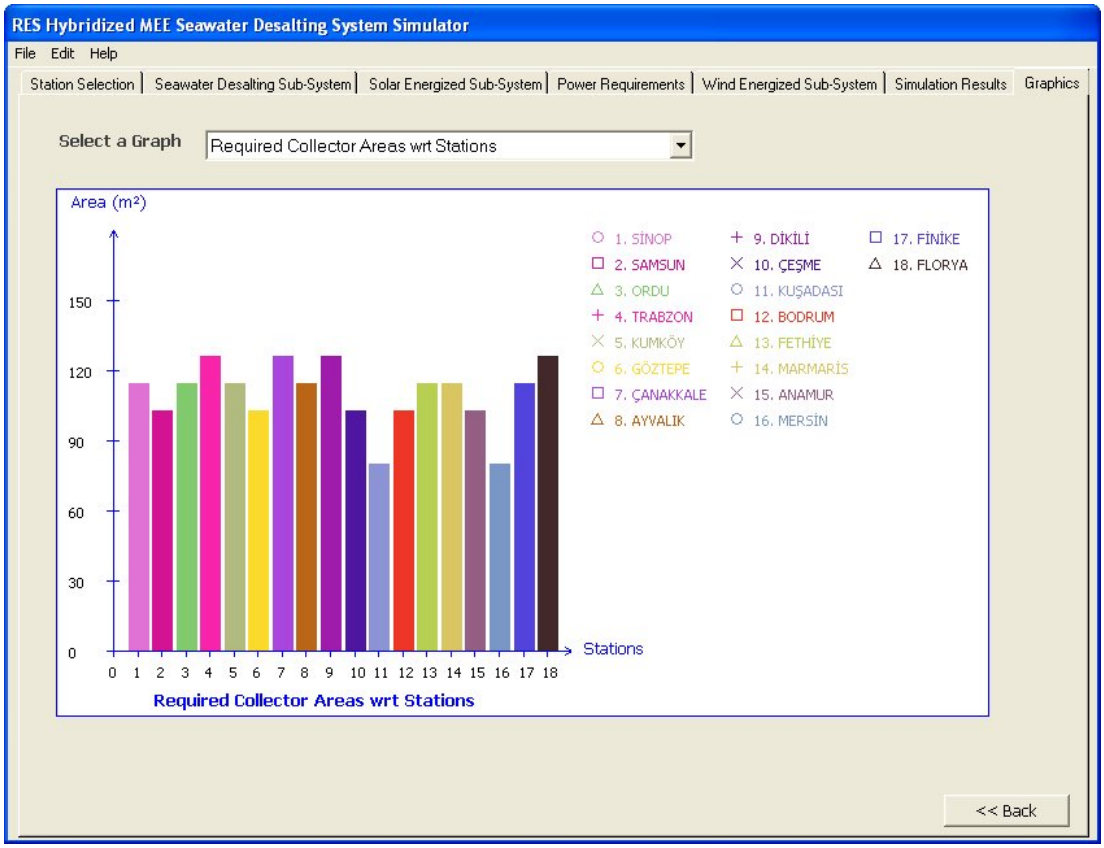

Figure 6.31 Required collector areas with respect to the stations

station. While determining the collector areas for each station, the maximum useful gain occurred in the year is calculated with the help of the sub-program. If the solar energy potential of the station is high, the calculated collector area will be getting lower. As it is seen from the figure, Kuşadası and Mersin have the lower collector areas among the stations.

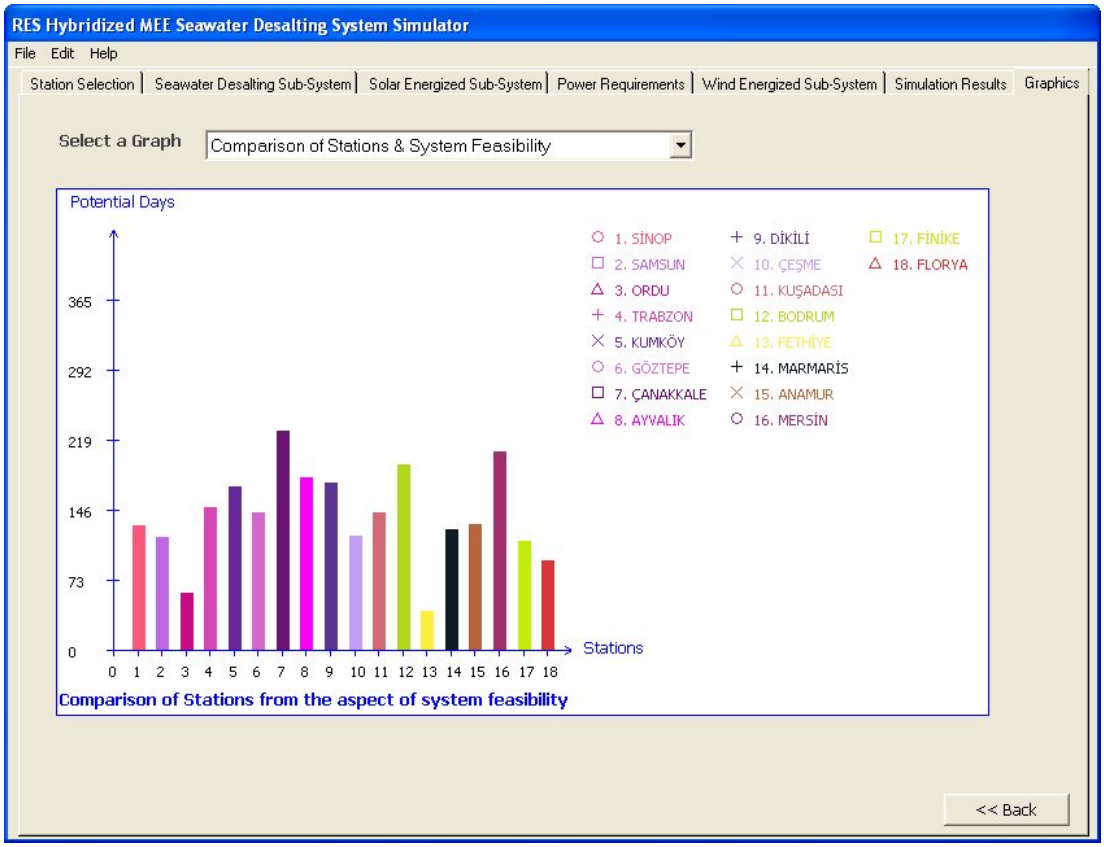

Figure 6.32 Comparison of the stations from the aspect of system feasibility

Figure (6.32) demonstrates the potential days of the total system from the point of view of design criteria for all stations. The potential days of each station are determined according to the design criteria and thus the potentials days passing the design criteria are summed and form the total. As it was explained before, these criteria depend on each other but the determination of the total potential day is initiated with the design min-temperature criterion at first. The remaining days left from the previous criterion are subjected to the second criterion and eventually the total potential day is determined. A station may have plenty of solar energy potential but have small amount of wind energy potential or vice versa or may have plenty of both of them. The station in Mersin has the lowest collector area and this means that

it has the highest solar energy potential. However its number of total potential day is lower than Çanakkale and this means that Çanakkale has higher wind energy potential according to Mersin and the other stations. The collector area required for the identical system design can be seen from the Fig. (6.31). The solar energized sub-system in Mersin has collector area which is lower than Çanakkale' nearly fifty percent. Furthermore, the turbine rotor areas used in these stations are the same. If it is considered for the same collector area and rotor area, the total potential day for Çanakkale will decrease and thus Mersin would pass on Çanakkale.

CHAPTER 7

CONCLUSIONS AND RECOMMENDATIONS

In this study, Multi-Effect Evaporation Seawater Desalination System Using Hybrid RES is designed and computer-simulated for 18 stations in Turkey. The simulations are performed by preparing a computer package in Visual Basic.

It is found that the results obtained from the system model are in accordance with literature. Some of the conclusions related with system simulation can be summarized as follows:

1. The performance ratio is nearly independent of the top brine temperature and is strongly related to the number of effects. In other words, the increase in the number of effects increases the performance ratio in MEE-FF desalination systems.

2. The specific heat transfer area increases by reducing the TBT and raising the number of effects.

3. The variation in the conversion ratio is constant and independent from the TBT. It depends only on intake seawater salinity and rejected brine salinity concentration in MEE-FF desalination systems.

4. The specific cooling water flow rate is nearly constant at different TBT values and decreases with the increase in the number of effects.

5. The change in cooling seawater temperature between 10°C and 25°C has negligible effect on the variation in cooling seawater mass flowrate while determining the design area of down condenser.

6. Even though evaporator tubes are faced with scaling problem at high TBTs, this problem can be eliminated at low TBTs and this also provide that the efficiency values of the collector series becomes relatively high with respect to high TBT for the constant temperature difference between collector outlet temperature and TBT to produce same amount of heating steam.

7. Seawater salinity concentration increases from the north to the south seas of Turkey. Low intake seawater salinity decreases scaling upon evaporator tubes. It would be reasonable to set up a system to onshore stations of Black sea if the renewable energy potential in this field were sufficient.

8. The solar energized sub-systems in Kuşadası and Mersin have the same and lowest collector areas however the potential days of Kuşadası coming from the solar energy availability have a lower value than Mersin. Mersin is the station which has the highest solar energy potential among 18 stations.

9. Despite the fact that Mersin has the highest solar energy potential day, Çanakkale has the highest total potential day among the stations on account of its highest wind energy potential.

10. Solar energy is more stable than wind energy owing to the fact that wind is a vectorial quantity; both speed and direction are required to define it. The fluctuations in the values of the wind velocity are higher than solar radiation flux during the day of the year. When setting-up of the total system in a station is considered, this knowledge should be taken into account. If this is considered Mersin will be the station from the view of system feasibility and applicability first of all.

11. Solar and wind types of renewable energies can be variable and intermittent during the time. Being able to overcome these problems two design criteria was developed and applied to the system. Feasibility comparison of stations is considered also for the identical collector areas, Mersin will be the most feasible one if all of the design criteria become equal.

12. In this study, flat plate collector and its mathematical modeling was used in throughout steam generation process. Other solar collector systems can be researched and compared from the view of system feasibility or economical analysis for further study.

13. Wind turbine rotor area can be optimized to meet the power requirement of the sub-systems during the system operation as a further study.

14. This simulation program covers only for the feasibility study of 18 stations in Turkey. If sufficient simulation data corresponding to other onshore stations of Turkey would be had, a further study could be made easily using this program package.

REFERENCES

[1]. El-Dessouky, H. T., Alatiqi, I. M., and Bingulac, S., and Ettouney, H. M. (1998). Steady-state analysis of the multiple effect evaporation desalination process, *Chemical Engineering & Technology*, **21**, 15–29.

[2]. Narmine H. Aly, Adel K. El-Fiqi (2003). Thermal performance of seawater desalination systems, *Desalination*, **158**, 127–142.

[3]. M.A. Darwish, Faisal Al-Juwayhel, Hassan K. Abdulraheim (2006). Multi-effect boiling systems from an energy viewpoint, *Desalination*, **194**, 22–39.

[4]. Hisham M. Ettouney, Hisham El-Dessouky (1999). A simulator for thermal desalination processes, *Desalination*, **125**, 277–291.

[5]. Hisham Ettouney (2004). Visual basic computer package for thermal and membrane desalination processes, *Desalination*, **165**, 393–408.

[6]. A.S. Nafeya, H.E.S. Fathb, A.A. Mabrouka (2006). A new visual package for design and simulation of desalination processes, *Desalination*, **194**, 281–296.

[7]. A. Jernqvista, M. Jernqvista, G. Alyb (2001). Simulation of thermal desalination processes, *Desalination*, **134**, 187–193.

[8]. E. E. Delyannis (1987). Status of solar assisted desalination: A rewiew, *Desalination*, **67**, 3–19.

[9]. Moh'd S. Abu-Jabal, I. Karniyab, Y. Namsakib (2001). Proving test for a solar-powered desalination system in Gaza-Palestine, *Desalination*, **137**, l–6.

[10]. Ali M. El-Nashar (1985). Abu Dhabi Solar Distillation Plant, *Desalination*, **52**, 217–234.

[11]. Soteris Kalogirou (1998). Use of parabolic trough solar energy collectors for sea-water desalination, Applied Energy, **60**, 65–88.

[12]. Bernhard Milowr and Eduardo Zarza (1996). Advanced MED solar desalination plants. Configurations, costs, future - seven years of experience at the Plataforma Solar de Almeria (Spain), Desalination, **108**, 51-58.

[13]. M. Al-Shammiri, M. Safar (1999). Multi-effect distillation plants: state of the art, *Desalination*, **126**, 45–59.

[14]. Lourdes Garcia-Rodriguez (2002). Seawater desalination driven by renewable energies: a review, *Desalination*, **143**, 103-l 13.

[15]. H.T. Eldessouky, H.M. Ettouney (2002). *Fundamentals of salt water desalination*. Amsterdam: Elsevier Science.

[16]. Çengel Y.A. (2003). *Heat Transfer*. (2nd ed.). New York: McGraw Hill.

[17]. Lourdes Garcia-Rodriguez, Ana I. Palmero-Marrero, Carlos Gomez-Camacho (2002). Comparison of solar thermal technologies for applications in seawater desalination, *Desalination*, **142**, 135–142.

[18]. J.A. Duffie, W.A. Beckman (1991). *Solar engineering of thermal processes* (2nd ed.). New York: John Wiley and Sons.

[19]. ASHRAE Standard 93 (1977). *Methods of testing to determine the thermal performance of solar collectors*. New York: American Society for Heating, Refrigeration, and Air -Conditioning Engineering.

[20]. *ASHRAE Handbook–HVAC systems and equipment* (2008). Atlanta: ASHRAE

[21]. http://www.windpower.org/en/tour/wres/cp.htm

[22]. Hau Erich (2006). *Wind Turbines: Fundamentals, Technologies, Application, Economics* (2nd ed.). New York: Springer.

[23]. R.C. Bansal, T.S. Bhatti, D.P. Kothari (2002). On some of the design aspects of wind energy conversion systems, *Energy Conversion and Management*, **43**, 2175–2187.

[24]. Thomas Ackermann, Lennart Söder (2002). An overview of wind energy-status, *Renewable and Sustainable Energy Reviews*, **6**, 67–128.

[25]. Demet Akgül, Mehmet Çakmakcı, Necati Kayaalp, İsmail Koyuncu (2008). Cost analysis of seawater desalination with reverse osmosis in Turkey, *Desalination*, **220**, 123–131.

APPENDICES

APPENDIX A

FORMULAS OF THE THERMODYNAMIC & HEAT TRANSFER PROPERTIES OF WATER AND SEAWATER

The table data for specific heat at constant pressure is approximated with the following formula [1]:

$$c_{p,w} = a + bT + cT^{1.5} + dT^2 + eT^{2.5} \tag{A1.1}$$

where $a = 4.2174356$, $b = -0.0056181625$, $c = 0.0012992528$, $d = -0.00011535353$, and $e = 4.14964 \times 10^{-6}$ are constants (with FitStdErr = 0.000696).

Saturation pressure of water can be calculated from the international equation and lately revised according to the International Temperature Scale (ITS-90) by [1]:

$$p_s = p_c \exp\left\{\left[T_c / (273.15 + T)\right]\left(a_1\tau + a_2\tau^{1.5} + a_3\tau^3 + a_4\tau^{3.5} + a_5\tau^4 + a_6\tau^{7.5}\right)\right\} \tag{A1.2}$$

where $p_c = 220.64$, the critical pressure of water; $T = 647.096$ K, the critical temperature of water, $\tau = 1 - (273.15 + T)/T_c$, $a_1 = -7.85951783$, $a_2 = 1.84408259$, $a_3 = -11.7866497$, $a_4 = 22.6807411$, $a_5 = -15.9618719$, and $a_6 = 1.80122502$. The above equation gives results within an uncertainty of ±0.025%.

The latest internationally accepted equation for the density of saturated ordinary water is provided by [1] in the form:

$$\rho_w = \rho_c\left(1 + b_1\tau^{1/3} + b_2\tau^{2/3} + b_3\tau^{5/3} + b_4\tau^{16/3} + b_5\tau^{43/3} + b_6\tau^{110/3}\right) \tag{A1.3}$$

where $\rho_c = 322$ kg/m³, the critical density of water, $b_1 = 1.99274064$, $b_2 = 1.09965342$, $b_3 = -0.510839303$, $b_4 = -1.75493479$, $b_5 = -45.5170352$, and $b_5 = -6.74694450 \times 10^{-5}$. This formula is accepted by the IAPWS and revised according to the International Temperature Scale of 1990 (ITS-90). Estimated tolerances of the most probable density between 0 and 150°C are determined from ±0.001%.to ±0.003%.

The seawater specific heat at constant pressure is given by the following correlation [2]:

$$c_{p,sw} = \left(A + BT + CT^2 + DT^3\right) \times 10^{-3} \qquad \text{(A1.4)}$$

where, the variables *A*, *B*, *C* and *D* are evaluated as a function of the water salinity as follows:

$$A = 4206.8 - 6.6197s + 1.2288 \times 10^{-2} s^2$$
$$B = -1.1262 + 5.4178 \times 10^{-2} s - 2.2719 \times 10^{-4} s^2$$
$$C = 1.2026 \times 10^{-2} - 5.3566 \times 10^{-4} s + 1.8906 \times 10^{-6} s^2$$
$$D = 6.8777 \times 10^{-7} + 1.517 \times 10^{-6} s - 4.4268 \times 10^{-9} s^2$$

where $c_{p,sw}$ in kJ/kg °C, T in °C, and s is the water salinity in gm/kg. The above correlation is valid over salinity and temperature ranges of $20000 \le X \le 160000$ ppm and $20 \le T \le 180$ °C, respectively.

The specific enthalpy of saturated water can be calculated with a relatively simple formula is proposed by [1]:

$$h_{fs} = d_1 + d_2 T + d_3 T^2 + d_4 T^3 + d_5 T^4 + d_6 T^5 \qquad \text{(A1.5)}$$

where $d_1 = -2.844699 \times 10^{-2}$, $d_2 = 4.211925$, $d_3 = -1.017034 \times 10^{-3}$, $d_4 = 1.311054 \times 10^{-5}$, $d_5 = -6.756469 \times 10^{-8}$, and $d_6 = 1.724481 \times 10^{-10}$. The

results of this formula in the range from 0.01 to 150°C deviate from the International Skeleton Tables (IST-85) by no more than ±0.013 kJ/kg. The uncertainty of the IST-85 tabulated data in this range of temperatures does not exceed ±0.057%.

The latent heat of vaporization of water is determined from an approximate formula [1]:

$$h_{fg} = a + bT + cT^{1.5} + dT^{2.5} + eT^{3} \tag{A1.6}$$

where $a = 2500.304$, $b = -2.2521025$, $c = -0.021465847$, $d = 3.1750136 \times 10^{-4}$, and $e = -2.8607959 \times 10^{-5}$ are constants (with FitStdErr = 0.0276). The estimated uncertainty of is approximately ±0.09%.

The boiling point elevation, *BPE*, is calculated from the following empirical formula [3]:

$$BPE = X\left(B + CX\right)10^{-3} \tag{A1.7}$$

with

$$B = \left(6.71 + 6.34 \times 10^{-2} T + 9.74 \times 10^{-5} T^{2}\right)10^{-3}$$

$$C = \left(22.238 + 9.59 \times 10^{-3} T + 9.42 \times 10^{-5} T^{2}\right)10^{-8}$$

where T is the temperature in °C and X is the salt concentration in ppm. The above equation is valid over the following ranges: $20000 < X < 160000$ ppm, $20 < T < 180$ °C.

The model developed by [3] gives the correlations for overall heat transfer coefficient values in evaporators and condenser, respectively. Furthermore the clean overall heat transfer coefficients by El-Dessouky et al. (1998) are the same with the Equations (A1.8) and (A1.9), where it uses a fouling resistance of 0.08 m²°C/kW.

Fouled evaporator correlation is donated as below,

$$U_e = 1961.9 + 12.6T - 9.6 \times 10^{-2} T^2 + 3.16 \times 10^{-4} T^3 \quad \text{(A1.8)}$$

Fouled condenser correlation is given in a similar manner

$$U_c = 1719.4 + 3.2T + 1.6 \times 10^{-2} T^2 - 2 \times 10^{-4} T^3 \quad \text{(A1.9)}$$

where, T, is the evaporation and condensation temperature.

APPENDIX B

BETZ'S ELEMENTARY MOMENTUM THEORY

The kinetic energy of an air mass m moving at a velocity v can be expressed as:

$$E = \frac{1}{2} m v^2 \qquad \text{(N.m)}$$

Considering a certain cross-sectional area A, through which the air passes at velocity v, the volume $\dot{V}$ flowing through during a certain time unit, the so-called volume flow, is:

$$\dot{V} = vA \qquad \text{(m}^3\text{/s)}$$

and the mass flow with the air density ρ is:

$$\dot{m} = \rho v A \qquad \text{(kg/s)}$$

The equations expressing the kinetic energy of the moving air and the mass flow yield the amount of energy passing through cross-section A per unit time. This energy is physically identical to the power P:

$$P = \frac{1}{2} \rho v^3 A \qquad \text{(W)}$$

The question is how much mechanical energy can be extracted from the free-stream airflow by an energy converter. As mechanical energy can only be extracted

at the cost of the kinetic energy contained in the wind stream, this means that, with an unchanged mass flow, the flow velocity behind the wind energy converter must decrease. Reduced velocity, however, means at the same time a widening of the cross-section, as the same mass flow must pass through it. It is thus necessary to consider the conditions in front of and behind the converter (Fig. B.1).

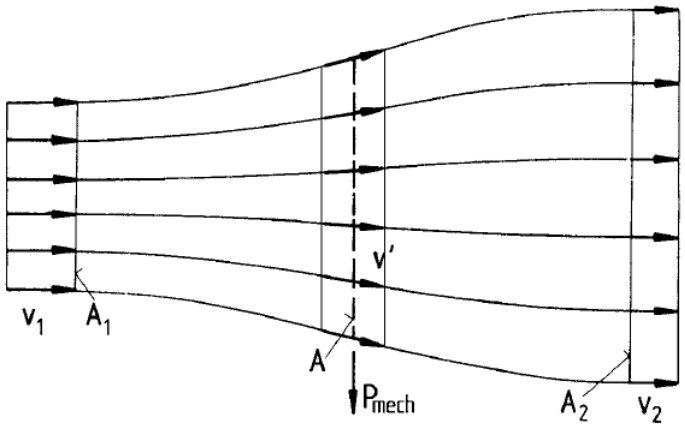

Figure B.1 Flow conditions due to the extraction of mechanical energy from a free-stream air flow, according to the elementary momentum theory

Here, v_1 is the undelayed free-stream velocity, the wind velocity, before it reaches the converter, whereas v_2 is the flow velocity behind the converter. The mechanical energy which the disk-shaped converter extracts from the airflow corresponds to the power difference of the air stream before and after the converter:

$$P = \frac{1}{2}\rho A_1 v_1^3 - \frac{1}{2}\rho A_1 v_2^3 = \frac{1}{2}\rho\left(A_1 v_1^3 - A_1 v_2^3\right) \qquad \text{(W)}$$

Maintaining the mass flow (continuity equation) requires that:

$$\rho v_1 A_1 = \rho v_2 A_2 \qquad \text{(kg/s)}$$

Thus,

$$P = \frac{1}{2}\rho A_1 v_1\left(v_1^2 - v_2^2\right) \qquad \text{(W)}$$

or

$$P = \frac{1}{2}\dot{m}\left(v_1^2 - v_2^2\right) \qquad \text{(W)}$$

From this equation it follows that, in purely formal terms, power would have to be at its maximum when v_2 is zero, namely when the air is brought to a complete standstill by the converter. However, this result does not make sense physically. If the outflow velocity v_2 behind the converter is zero, then the inflow velocity before the converter must also become zero, implying that there would be no more flow through the converter at all. As could be expected, a physically meaningful result consists in a certain numerical ratio of v_2/v_1 where the extractable power reaches its maximum.

This requires another equation expressing the mechanical power of the converter. Using the law of conservation of momentum, the force which the air exerts on the converter can be expressed as:

$$F = \dot{m}\left(v_1 - v_2\right) \qquad \text{(N)}$$

According to the principle of “action equals reaction”, this force, the thrust, must be counteracted by an equal force exerted by the converter on the airflow. The thrust, so to speak, pushes the air mass at air velocity v', present in the plane of flow of the converter. The power required for this is:

$$P = Fv' = m\left(v_1 - v_2\right)v' \qquad \text{(W)}$$

Thus, the mechanical power extracted from the air flow can be derived from the energy or power difference before and after the converter, on the one hand, and, on the other hand, from the thrust and the flow velocity. Equating these two expressions yields the relationship for the flow velocity v':

$$\frac{1}{2}\dot{m}\left(v_1^2 - v_2^2\right) = \dot{m}\left(v_1 - v_2\right)v' \quad \text{(W)}$$

$$v' = \frac{1}{2}(v_1 - v_2) \qquad \text{(m/s)}$$

Thus the flow velocity through the converter is equal to the arithmetic mean of v_1 and v_2:

$$v' = \frac{v_1 + v_2}{2} \qquad \text{(m/s)}$$

The mass flow thus becomes:

$$\dot{m} = \rho A v' = \frac{1}{2}\rho A (v_1 + v_2) \quad \text{(kg/s)}$$

The mechanical power output of the converter can be expressed as:

$$P = \frac{1}{4}\rho A\left(v_1^2 - v_2^2\right)(v_1 + v_2) \quad \text{(W)}$$

In order to provide a reference for this power output, it is compared with the power of the free-air stream which flows through the same cross-sectional area A, without mechanical power being extracted from it. This power was:

$$P_0 = \frac{1}{2}\rho v_1^3 A \qquad \text{(W)}$$

The ratio between the mechanical power extracted by the converter and that of the undisturbed air stream is called the "power coefficient" c_P:

$$c_P = \frac{P}{P_0} = \frac{\frac{1}{4}\rho A\left(v_1^2 - v_2^2\right)(v_1 + v_2)}{\frac{1}{2}\rho v_1^3 A}$$

After some re-arrangement, the power coefficient can be specified directly as a function of the velocity ratio v_2/v_1 :

$$c_P = \frac{P}{P_0} = \frac{1}{2}\left|1-\left(\frac{v_2}{v_1}\right)^2\right|\left|1+\frac{v_2}{v_1}\right|$$

The power coefficient, i.e. the ratio of the extractable mechanical power to the power contained in the air stream, therefore, now only depends on the ratio of the air velocities before and after the converter. Differentiating the above equation with respect to v_2/v_1 and setting it to zero gives the optimum value of v_2/v_1 for maximum power output and solving the quadratic equation:

$$\frac{v_2}{v_1} = \frac{1}{3}$$

With $v_2/v_1 = 1/3$, the maximum "ideal power coefficient" c_P becomes

$$c_P = \frac{16}{27} = 0.593$$

Betz was the first to derive this important value and it is, therefore, frequently called the "Betz factor".